

The binary fraction, separation distribution, and merger rate of white dwarfs from SPY

Dan Maoz¹★ and Na’ama Hallakoun^{1,2}

¹*School of Physics and Astronomy, Tel-Aviv University, Tel-Aviv 6997801, Israel*

²*European Southern Observatory, Karl-Schwarzschild-Straße 2, D-85748 Garching, Germany*

Accepted XXX. Received YYY; in original form ZZZ

ABSTRACT

From a sample of spectra of 439 white dwarfs (WDs) from the ESO-VLT Supernova-Ia Progenitor survey (SPY), we measure the maximal changes in radial-velocity (ΔRV_{\max}) between epochs (generally two epochs, separated by up to 470 d), and model the observed ΔRV_{\max} statistics via Monte-Carlo simulations, to constrain the population characteristics of double WDs (DWDs). The DWD fraction among WDs is $f_{\text{bin}} = 0.100 \pm 0.020$ (1σ , random) $+0.02$ (systematic), in the separation range $\lesssim 4$ AU within which the data are sensitive to binarity. Assuming the distribution of binary separation, a , is a power-law, $dN/da \propto a^\alpha$, at the end of the last common-envelope phase and the start of solely gravitational-wave-driven binary evolution, the constraint by the data is $\alpha = -1.3 \pm 0.2$ (1σ) ± 0.2 (systematic). If these parameters extend to small separations, the implied Galactic WD merger rate per unit stellar mass is $R_{\text{merge}} = (1 - 80) \times 10^{-13} \text{ yr}^{-1} M_{\odot}^{-1}$ (2σ), with a likelihood-weighted mean of $R_{\text{merge}} = (7 \pm 2) \times 10^{-13} \text{ yr}^{-1} M_{\odot}^{-1}$ (1σ). The Milky Way’s specific Type-Ia supernova (SN Ia) rate is likely $R_{\text{Ia}} \approx 1.1 \times 10^{-13} \text{ yr}^{-1} M_{\odot}^{-1}$ and therefore, in terms of rates, a possibly small fraction of all merging DWDs (e.g. those with massive-enough primary WDs) could suffice to produce most or all SNe Ia.

Key words: binaries:close, spectroscopic – white dwarfs – supernovae: general

1 INTRODUCTION

A large fraction of all stars, and a majority of intermediate-mass and massive stars, are in multiple systems. Multiplicity is an outcome of star formation and early stellar evolution, and thus serves as a probe of those poorly understood processes. Furthermore, binary, triple, and higher-order systems provide the settings for a rich variety of astrophysical phenomena, including interacting, accreting, and merging binaries, various types of supernovae, and gravitational wave sources. However, the demographics of stellar multiplicity are still poorly known, i.e. the distribution of multiplicity index (single, binary, triple...), separation, component mass ratio, and eccentricity, all as a function of stellar mass, age, metallicity, and Galactic environment (e.g., Duquennoy & Mayor 1991; Raghavan et al. 2010). These demographics must be physically linked, at some level, to those of sub-stellar companions – brown dwarfs (BDs) and planets – for which our knowledge is even sketchier, and also to those of stellar remnants – white dwarfs (WDs), neutron stars, and black holes.

Binarity in WDs is particularly interesting. WDs are the end state of 95% of all stars, and they are the current state of the majority of all stars ever formed with mass above $1.2 M_{\odot}$. As such, binary WDs provide a fossil probe of the initial binary populations and of

their subsequent binary evolution. Systems consisting of close double WDs (DWDs) are potential progenitors of Type-Ia supernovae (SNe Ia; e.g. Maoz et al. 2014), AM Canum Venaticorum systems (a WD accreting from another degenerate or semi-degenerate companion star), and R Corona Borealis stars (highly magnetic WDs postulated to result from WD mergers; e.g. Longland et al. 2011). DWDs will be the main foreground of space-based gravitational-wave detectors such as LISA, both as resolved sources at higher gravitational-wave frequencies, and as an unresolved continuum at lower frequencies. Identifying the individual nearby DWD systems and measuring the binary parameter distribution as a whole for DWDs is therefore important for the budding field of gravitational-wave astronomy. Like other double-compact-remnant binaries (including neutron stars and black holes), DWDs are physically simple and “clean” systems in which the evolution of each WD is decoupled from the other WD and driven mainly by cooling via thermal emission from the surface, while the binary evolution is dictated solely by gravitational wave emission (except in the very final merger phases).

Systematic searches for DWDs began in the 1980s (see Napiwotzki et al. 2004, and references therein). There are now over 90 individual close DWD systems for which orbital parameters have been derived (see, e.g., Nelemans et al. 2005; Marsh 2011; Debes et al. 2015; Hallakoun et al. 2016; Brown et al. 2016, and references therein). Excluding systems with extremely low-mass

★ E-mail: maoz@astro.tau.ac.il (DM)

(ELM) WDs of $\sim 0.2 M_{\odot}$, which are found to be always in binaries, there are about 30 DWD systems with orbital parameters. The statistics of the short-orbit DWD population as a whole were examined by [Maxted & Marsh \(1999\)](#), who studied a sample of 46 WDs and estimated a binary fraction between 1.7% and 19%. More recently, [Maoz et al. \(2012, hereafter M12\)](#) developed a statistical method to characterize the DWD population in a sample of WDs, by measuring the distribution of ΔRV_{\max} , the maximum radial velocity (RV) shift between several epochs (two or more) of the same WD. M12 showed that even with just two epochs per WD and with noisy RV measurements, the ΔRV_{\max} distribution can set meaningful constraints on the binary fraction of the population, f_{bin} , and on the distribution of binary separations, dN/da . The ΔRV_{\max} method applied to such data permits also an estimate of the merger rate of the DWD population. Statistical inference about the DWD population is thus possible without follow-up observations and full binary parameter solutions for candidates.

[Badenes & Maoz \(2012, hereafter BM12\)](#) measured few-epoch RVs in the spectra of ~ 4000 WDs from the Sloan Digital Sky Survey (SDSS) and applied the method to the observed ΔRV_{\max} distribution. The data constrained f_{bin} at separations $a < 0.05$ AU to a 1σ range of 3 – 20%. Assuming a power-law separation distribution, $dN/da \propto a^{\alpha}$, at the time of DWD formation (from hence the binary separation evolves solely via gravitational-wave emission), M12 and BM12 showed that α is constrained to the range -2 to $+1$, with strong covariance between f_{bin} and α (low f_{bin} together with a steep negative power-law slope α , or a higher f_{bin} together with a shallower α , can both populate the small separation range with DWD systems and produce the high- ΔRV_{\max} tail in the observed distribution). As every combination of f_{bin} and α translates to a WD merger rate, BM12 showed that the WD merger rate per unit stellar mass in the Milky Way is constrained to $R_{\text{merge}} = 1.4_{-1}^{+3.4} \times 10^{-13} \text{ yr}^{-1} M_{\odot}^{-1}$, a range that straddles the Galactic SN Ia rate per unit stellar mass, $R_{\text{Ia}} \approx 1.1 \times 10^{-13} \text{ yr}^{-1} M_{\odot}^{-1}$. (The Milky Way’s specific SN Ia rate can be reliably estimated from its approximate mass and from the fact that it is an Sbc galaxy; see BM12).

The SDSS sample of WDs analysed by M12 and BM12, while large, suffered from a low RV precision of $\sim 80 \text{ km s}^{-1}$, a result mainly of the low resolution of the SDSS spectra and of the fact that most WDs have only a few, highly Stark-broadened hydrogen Balmer absorption lines in their spectra. As a consequence, only the systems in the sample with observed $\Delta RV_{\max} \geq 250 \text{ km s}^{-1}$ (some 15 in number) drove the statistical conclusions. This lower limit in the significantly detectable ΔRV_{\max} translated, for typical WD masses, to an upper limit in the binary separation that is probed by the study, of $a \sim 0.05$ AU. Furthermore, the small number of systems driving the signal results in large statistical errors and in the strong degeneracy between the model parameters.

In the present paper, we apply the method of M12 and BM12 to another sample of multi-epoch WD spectra, from the European Southern Observatory (ESO), 8 m Very Large Telescope (VLT), Supernova-Ia Progenitor survey (SPY; [Napiwotzki et al. 2001](#)). SPY was a few-epoch spectroscopic survey of ~ 800 bright ($V \sim 16$ mag) WDs, with the objective of using RV differences between epochs to identify close DWD systems that will merge within a Hubble time, thus being potential SN Ia progenitors. Published results from SPY relevant to DWDs include [Napiwotzki et al. \(2002\)](#) (discovery of a DWD with a mass close to the Chandrasekhar limit); [Karl et al. \(2003a,b\)](#) (follow-up analysis of several DWDs); [Nelemans et al. \(2005\)](#) (follow-up analysis of five DWDs from SPY); and [Koester et al. \(2009\)](#) (catalogue and spectroscopic anal-

ysis of hydrogen-dominated WDs, including a list of DWDs). A statistical analysis of the SPY dataset as a whole, and its implications for the binary WD population, has not been published to date.

Out of the full SPY dataset, we select about 500 WDs suitable for our present analysis. Although the sample size is an order of magnitude smaller than the SDSS WD sample of BM12, the high spectral resolution and signal-to-noise ratio (S/N) possible with the VLT permit resolving the narrow non-local-thermodynamic equilibrium (NLTE) core of the $H\alpha$ line (and sometimes $H\beta$) that exists in the spectra of DA-type WDs (i.e. WDs with only hydrogen lines in their optical spectra, which constitute the majority of WDs). This provides a typical RV resolution of $1 - 2 \text{ km s}^{-1}$ per epoch, a factor ~ 50 times better than for the SDSS sample. This RV resolution, combined with the distribution of time separations between epochs in SPY, means that the SPY sample is sensitive to DWDs out to separations $a \sim 4$ AU (see Section 3, below). While, in principle, the lowest-separation/highest-RV systems are also detectable in SPY, the small sample size of SPY makes it unlikely to “catch” those systems, and in fact the largest ΔRV_{\max} that we measure is 240 km s^{-1} . The SPY sample thus nicely complements the SDSS sample, in so much as it probes the WD population’s binarity in the $a = 0.05 - 4$ AU interval range, compared to the $a = 0.001 - 0.05$ AU range probed by SDSS (the lower limit in SDSS arising from the exposure length of ~ 15 min, which prevents the detection of RV variations in systems with orbital periods comparable to this time.) The logarithmic interval in separation probed, in principle, by SPY, $a = 0.001 - 4$ AU, is 2.1 times larger than the $a = 0.001 - 0.05$ AU logarithmic interval of SDSS. Therefore, for example, for a separation distribution that has equal numbers of binaries per logarithmic interval, one would expect to find a binarity fraction about twice as high in SPY as in SDSS.

From analysis of the SPY sample, below, we find values of f_{bin} , α , and the merger rate of the WD population, that are consistent with the findings of BM12 for the SDSS sample, but are now more tightly constrained. The allowed values of α and R_{merge} strengthen the case for the “double-degenerate” progenitor scenario of SNe Ia.

2 WD SAMPLE AND RV MEASUREMENT

The full SPY sample includes some 2200 spectra of about 800 WDs that were observed between the years 2001 and 2003 with the UV-Visual Echelle Spectrograph (UVES) of the ESO Very Large Telescope (VLT). The SPY program setup used UVES in a dichroic mode, covering most of the range between 3200 \AA and 6650 \AA , with two $\sim 80 \text{ \AA}$ gaps around 4580 \AA and 5640 \AA ([Napiwotzki et al. 2003](#)). The spectral resolution is at least $R = 18500$ (0.36 \AA at $H\alpha$). A S/N per binned pixel (0.03 \AA) of ≥ 15 was achieved using 5 – 10 min exposures. The SPY WDs were selected from a number of WD compilations and catalogues: the [McCook & Sion \(1999\)](#) catalogue of spectroscopically confirmed WDs; the Hamburg-ESO survey (HES; [Wisotzki et al. 1996](#); [Christlieb et al. 2001](#)); the Hamburg-Quasar survey (HQS; [Hagen et al. 1995](#)); the Montreal-Cambridge-Tololo survey (MCT; [Demers et al. 1990](#); [Lamontagne et al. 2000](#)); and the Edingburgh-Cape survey (EC; [Kilkenny et al. 1991](#)). The SPY targets were selected to have $B \leq 16.5$ mag and declination $\delta \leq +25^{\circ}$. Each WD was observed on several epochs (typically two, although in many cases one of the two epochs has noisy data, leaving effectively just one epoch, from which it is impossible to find RV changes, see below). The ~ 800 SPY WDs include 615 WDs of type DA

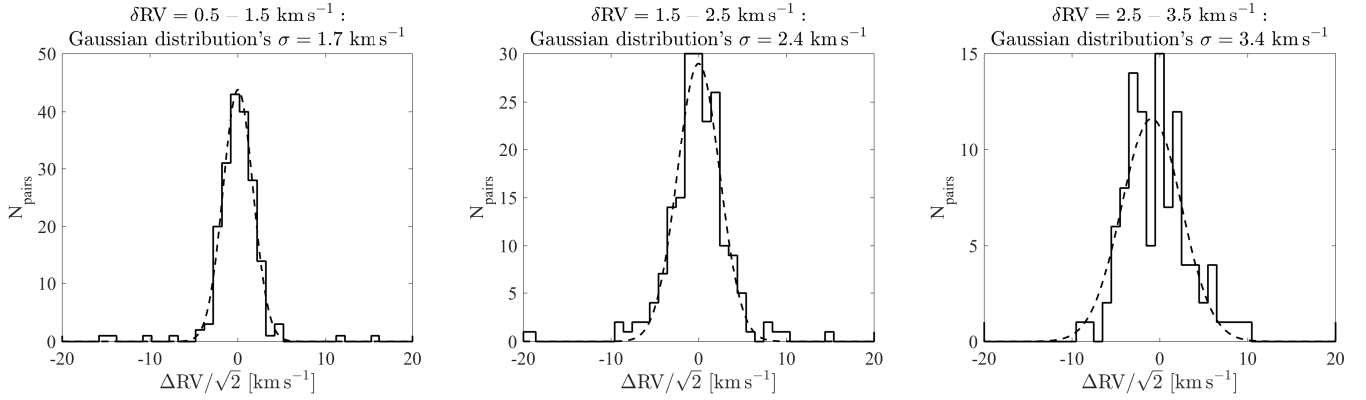


Figure 1. Distributions of observed ΔRV differences between two epochs of observations of the same WDs, scaled down by $\sqrt{2}$, and Gaussian fits to the distributions (dashed), for pairs of measurements having pair-averaged formal RV fitting errors of $0.5\text{--}1.5\text{ km s}^{-1}$ (left), $1.5\text{--}2.5\text{ km s}^{-1}$ (center), and $2.5\text{--}3.5\text{ km s}^{-1}$ (right). Except for some outlier points, resulting from real DWD systems, the distributions appear Gaussian with a σ close to the expected value, indicating that the formal RV errors from the Balmer line-profile fitting are reliable.

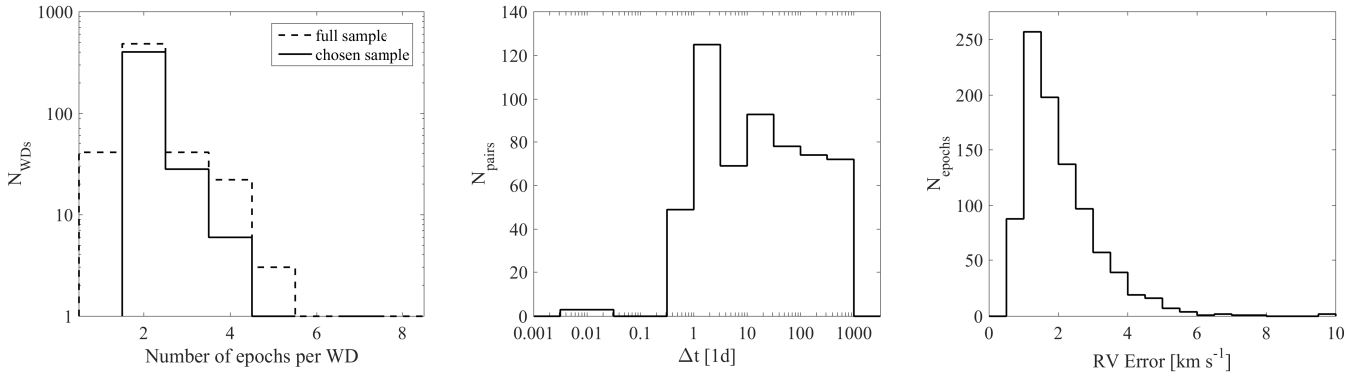


Figure 2. Left: the distribution of the number of epochs per WD, for all SPY DA WDs (dashed line) and for our final (solid line) sample. Centre: the distribution of time differences between epochs, for all epochs in the final sample. Right: the distribution of RV errors in the sample.

(with spectra dominated by hydrogen Balmer absorption lines, see Koester et al. 2009), 46 DA+dM binaries (Koester et al. 2009), 10 DAH (magnetic DAs, see Koester et al. 2009), 71 DB or DBA WDs (with helium lines, see Voss et al. 2007), 24 DAZ WDs (DA WDs with photospheric metal lines, generally Ca II), 25 DAs with interstellar metal lines, and 17 helium-rich WDs with metal lines (Koester et al. 2005). As the majority of the sample are DAs, which have the sharp NLTE Balmer-line cores that permit the highest RV accuracy, we focus from here on only on a uniform sample consisting of the DA and DAZ WDs in the sample.

Falcon et al. (2010) have measured RVs in individual SPY spectra of single DA WDs for the purpose of gravitational-redshift estimation, and we have adopted their methodology, as follows. We fitted a region of $\pm 500\text{ km s}^{-1}$ around the position of the $H\alpha$ NLTE line core with a combination of a Gaussian (fitting the NLTE core) and a parabola (fitting the local region of the full line profile), using least-squares, with RV error estimates for every fit obtained based on the covariance matrix from the fit. All velocities were barycentre-corrected using the correction values provided by the UVES pipeline. All fitted spectra were inspected by eye, and 238 epochs of 135 WDs with problematic fits due to noisy or flawed data were excluded from the sample. To optimise the statistical power of our sample, a further three spectra of three WDs having formal RV errors $> 10\text{ km s}^{-1}$ were excluded from the sample.

To examine the reliability of the RV error estimates (which is

important for our Monte Carlo simulation of the results, Section 3, below), we have compared the mean RV error estimate from every pair of epochs for the same WD, to the actual RV difference between those epochs, scaled down by $\sqrt{2}$. As the majority of the WDs in the sample are single (or their binary nature is not revealed by these observations), the scaled-down ΔRV values for all WDs having a given RV error estimate from the fitting process should follow a Gaussian distribution, centred on zero and with a σ corresponding to the RV error estimate, except for some high ΔRV outliers due to the minority of DWDs with real RV changes between epochs. Good agreement with this expectation is indeed reflected in Figure 1, which shows the distributions of observed RV epoch differences for several narrow ranges of the formal RV errors. From this comparison, the formal RV errors possibly underestimate the true RV errors by $\sim 0.5\text{ km s}^{-1}$. Thus, we have taken 0.5 km s^{-1} as the minimal error and updated the measured errors accordingly. The $H\beta$ NLTE line core in the spectra is not always clearly detected and gives a noisier RV measurement, and hence we rely only on $H\alpha$ for our RVs.

In most spectroscopic DWD binaries, the light from one of the WDs is dominant, and therefore the binary is single-lined. However, 14 of the DA WDs are double-lined, with clearly separated NLTE line cores. In those cases we have fitted the region around the double NLTE core with a combination of two Gaussians and a parabola. All but a handful of the WDs have time differences be-

tween epochs of up to 470 d, and this time difference dictates the range of orbital separations to which the sample is sensitive. We have therefore excluded from the sample epochs separated by more than 470 d from any other epoch. Finally, the maximal velocity difference between any two epochs for every WD, ΔRV_{\max} , was calculated for the final sample. In the case of double-lined systems, with two RV values per epoch, the RV value used for the calculation was that of the deeper NLTE core, or chosen randomly if both NLTE cores were of the same depth.

Our final sample consists 926 spectra of 439 WDs that have more than one epoch each. Figure 2 shows the distribution of the number of epochs per WD, the distribution of time differences between epochs, and the distribution of RV errors.

Figure 3 presents the main observed statistic of this work, the distribution of ΔRV_{\max} , the maximal velocity difference between any two epochs for every WD. The dashed curve shows the expected ΔRV_{\max} distribution from a Monte-Carlo simulation (Section 3, below) of a sample in which there are *no* binaries, and therefore all observed RV changes in this simulated distribution result solely from measurement noise. One can see that, above $\Delta RV_{\max} \gtrsim 10 \text{ km s}^{-1}$, real WD binaries dominate the distribution.

Table A1 lists the parameters and RV measurements for the full final WD sample. Table 1 collects only the 43 candidate DWD systems having $\Delta RV_{\max} > 10 \text{ km s}^{-1}$, which are also highlighted in Table A1.

A pertinent question at this point is the nature of the companions in the candidate binary systems in the tail of the ΔRV_{\max} distribution. We argue that all but one or two, at most, are also WDs (i.e. the systems are DWDs). Main-sequence companion stars that are hot enough would reveal themselves in the red regions of the SPY spectra by means of their molecular-band features. Indeed, as noted above, Koester et al. (2009) already identified in this way 46 WD+dM systems in the SPY sample, which we have excluded from our analysis. Among the ΔRV_{\max} tail WDs, the most luminous one has absolute R magnitude $M_R \sim 9.7$. An M3 companion star of effective temperature $T_{\text{eff}} \approx 3300 \text{ K}$ and mass $\sim 0.2 M_{\odot}$ has $M_R \sim 11.2 \text{ mag}$ (Baraffe & Chabrier 1996), only a factor of 4 fainter than the WD, and hence would likely still be detected in the SPY spectrum.

To test for the presence of cooler stellar and sub-stellar companions, we have examined on VizieR (Ochsenbein et al. 2000) the available optical to near-infrared (NIR) photometry, including the spectrophotometrically calibrated SPY spectra themselves, for all of the 43 “tail” WDs. To the optical-band photometry of each WD, we have fit a scaled Planck spectrum with a temperature according to the WD’s photospheric fit from Koester et al. (2009), corrected for the three-dimensional effects of convection using Tables B.5 and B.6 of Tremblay et al. (2013). We then searched for evidence of any NIR excess at $1 - 5 \mu\text{m}$ as indicated by the photometry from 2MASS (Skrutskie et al. 2006), UKIDSS (Lawrence et al. 2007), VISTA (Jarvis et al. 2013; Edge et al. 2013) and WISE (Cutri et al. 2014). To quantify any detected excesses and estimate the detection limits for excesses, we added to each model WD thermal spectrum a second thermal spectrum of varying temperature, scaled according to the ratio of the surface areas of the WD and of a $R = 0.1 R_{\odot}$ companion (appropriate for a low-mass star or BD). Each WD’s radius was based on the effective temperature and surface gravity calculated by Koester et al. (2009), corrected for 3D convection (Tremblay et al. 2013), and the theoretical WD

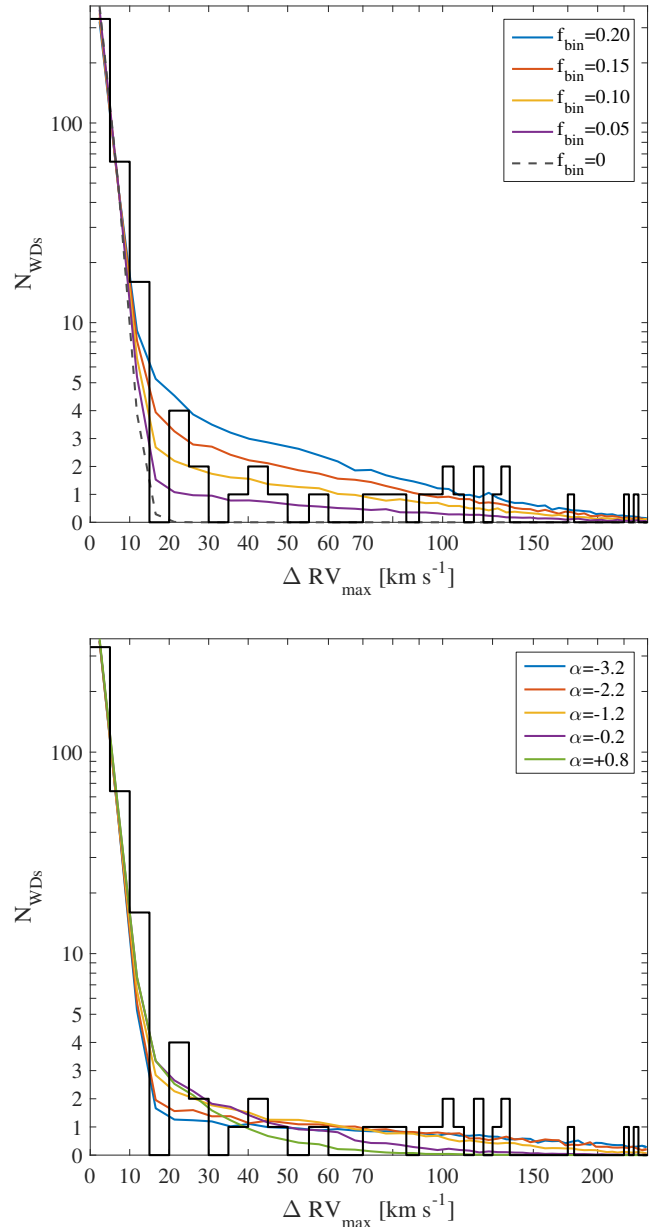


Figure 3. Distribution of ΔRV_{\max} (black histogram), compared to Monte-Carlo model distributions (coloured solid curves). Top: model dependence on binary fraction, f_{bin} , for a fixed $\alpha = -1.2$ value. The dashed black curve is a model with no DWDs ($f_{\text{bin}} = 0$). Bottom: model dependence on separation distribution power-law index, α , for a fixed $f_{\text{bin}} = 0.10$ value.

cooling sequences of Fontaine et al. (2001)¹. From the data, we estimate that we can detect a $\gtrsim 1500 \text{ K}$ NIR excess in the spectra of the hotter WDs in the sample, and $\gtrsim 1000 \text{ K}$ in the cooler WDs.

In four cases do we see an actual possible NIR excess. In three of these, the excess corresponds to a companion temperature of $\sim 1000 - 2000 \text{ K}$, i.e. a BD companion. However, two of these three cases, WD0037-006 and HE0410-1137, are double-lined DWDs, and the excess may be coming from the cooler of the two WDs in each system. Furthermore, in the double-lined spectra of these two WDs, the photometric temperature fit to the Balmer line profiles is

¹ <http://www.astro.umontreal.ca/~bergeron/CoolingModels/>

Table 1. Candidate DWDs with $\Delta RV_{\max} > 10 \text{ km s}^{-1}$.

Name	RA	Dec	Δt [d]	ΔRV_{\max} [km s^{-1}]	σ [km s^{-1}]	N_{σ}	M_1 [M_{\odot}]	Comments
HE1414-0848	14:16:52.07	-09:02:03.8	395.9	238.4	4.2	57.3	0.40	1, 2
WD2020-425	20:23:59.57	-42:24:26.7	23.0	225.9	2.9	77.3	0.75	1
WD0326-273	03:28:48.81	-27:19:01.7	3.0	179.3	1.2	151.2	0.35	3
WD1210+140	12:12:33.89	+13:46:25.1	0.9	133.1	1.8	72.6	0.30	4
WD0135-052	01:37:59.40	-04:59:44.9	4.0	132.4	0.8	159.3	0.20	1, 5
WD0037-006	00:40:22.94	-00:21:31.1	45.0	128.5	1.1	118.2	0.55	1
WD0341+021	03:44:10.77	+02:15:29.9	201.2	117.1	2.6	44.7	0.30	
WD0028-474	00:30:47.16	-47:12:36.9	59.8	116.8	1.7	67.1	0.50	1
HE2209-1444	22:12:18.05	-14:29:48.0	287.1	106.3	1.4	75.5	0.60	1, 6
WD2200-136	22:03:35.63	-13:26:49.9	368.1	104.0	4.7	22.3	0.45	1
WD1124-018	11:27:21.33	-02:08:37.7	1.9	101.9	3.0	34.0	0.50	
WD1824+040	18:27:13.13	+04:03:45.9	83.7	96.7	1.1	88.2	0.35	7
WD0344+073	03:46:51.42	+07:28:01.9	215.3	91.3	1.5	60.2	0.35	
WD1349+144	13:51:54.06	+14:09:44.2	1.1	84.3	2.7	30.7	0.55	1, 8
HS1102+0934	11:04:36.76	+09:18:22.7	320.9	77.1	1.7	45.9	0.45	9
HE0320-1917	03:22:31.91	-19:06:47.8	1.0	70.4	1.2	61.1	0.30	10
WD2330-212	23:32:59.48	-20:57:12.1	2.9	55.5	2.6	21.8	0.40	
HE0225-1912	02:27:41.43	-18:59:24.5	7.1	48.1	3.1	15.5	0.55	1
WD2336-187	23:38:52.78	-18:26:11.9	3.0	42.1	5.8	7.3	0.25	1
HE0410-1137	04:12:28.99	-11:30:08.3	4.0	40.9	1.4	28.7	0.50	1
WD0032-317	00:34:49.82	-31:29:54.3	1.0	38.1	3.8	10.1	0.35	11
WD1013-010	10:16:07.01	-01:19:18.7	20.9	29.0	2.3	12.6	0.25	12
HE0325-4033	03:27:43.92	-40:23:26.1	0.9	26.8	1.5	17.4	0.55	
HS2046+0044	20:48:38.26	+00:56:00.8	16.9	23.8	3.8	6.2	0.70	
HE0516-1804	05:19:04.27	-18:01:29.1	1.0	22.3	2.7	8.2	0.55	13
HE0131+0149	01:34:28.46	+02:04:21.4	392.9	21.6	1.3	16.2	0.50	
HE0324-1942	03:27:05.02	-19:32:23.8	0.9	21.4	3.7	5.8	0.80	1
HE0221-0535	02:23:59.88	-05:21:45.9	0.9	14.3	2.0	7.3	0.60	
WD1233-164	12:36:14.02	-16:41:53.5	270.3	14.1	3.9	3.7	0.75	
HE0221-2642	02:23:29.40	-26:29:19.7	226.3	14.0	5.9	2.4	0.55	
HS1334+0701	13:36:33.67	+06:46:26.8	309.2	13.1	2.0	6.5	0.40	
WD2359-324	00:02:32.36	-32:11:50.7	2.1	12.6	3.0	4.2	0.55	
WD2253-081	22:55:49.49	-07:50:03.3	5.0	12.4	1.7	7.5	0.20	
HS2216+1551	22:18:57.15	+16:06:56.9	1.1	12.4	1.9	6.4	0.65	1
HE0031-5525	00:33:36.03	-55:08:37.5	222.2	12.2	4.6	2.7	0.45	
HE2148-3857	21:51:19.23	-38:43:04.5	1.0	11.5	4.0	2.9	0.70	
WD2308+050	23:11:18.05	+05:19:27.9	1.0	11.4	4.3	2.7	0.45	
WD2254+126	22:56:46.26	+12:52:49.9	34.8	11.4	4.9	2.3	0.55	
HS1204+0159	12:07:29.51	+01:42:50.6	1.0	11.3	4.2	2.7	0.50	
HE0344-1207	03:47:06.71	-11:58:08.5	1.0	11.1	3.1	3.5	0.55	
WD0114-605	01:16:19.55	-60:16:07.6	343.0	10.9	2.4	4.6	0.50	
HE0417-3033	04:19:22.07	-30:26:44.0	261.2	10.2	3.1	3.3	0.50	
WD2248-504	22:51:02.02	-50:11:31.8	7.0	10.1	2.8	3.6	0.60	

Notes: σ is the root of the summed squares of the RV errors of the two individual RV measurements forming each difference. N_{σ} is defined as $\Delta RV_{\max}/\sigma$. M_1 is the derived mass for the photometric-primary WD.

(1) Double-lined DWD (2) HE1414-0848: $P = 0.5178 \text{ d}$, $M_1 = 0.55 M_{\odot}$, $M_2 = 0.71 M_{\odot}$ (Napiwotzki et al. 2002) (3) WD0326-273: $P = 1.8754 \text{ d}$, $M_1 = 0.51 M_{\odot}$, $M_{2,\min} = 0.59 M_{\odot}$ (Nelemans et al. 2005) (4) WD1210+140: $P = 0.64194 \text{ d}$, $M_1 = 0.23 M_{\odot}$, $M_{2,\min} = 0.38 M_{\odot}$ (Nelemans et al. 2005) (5) WD0135-052: $P = 1.553 \text{ d}$, $M_1 = 0.47 M_{\odot}$, $M_2 = 0.52 M_{\odot}$ (Saffer et al. 1988; Bergeron et al. 1989) (6) HE2209-1444: $P = 0.2769 \text{ d}$, $M_1 = 0.58 M_{\odot}$, $M_2 = 0.58 M_{\odot}$ (Karl et al. 2003b) (7) WD1824+040: $P = 6.26600 \text{ d}$, $M_1 = 0.428 M_{\odot}$, $M_{2,\min} = 0.515 M_{\odot}$ (Morales-Rueda et al. 2005) (8) WD1349+144: $P = 2.2094 \text{ d}$, $M_1 = 0.44 M_{\odot}$, $M_2 = 0.44 M_{\odot}$ (Karl et al. 2003a) (9) HS1102+0934: $P = 0.55319 \text{ d}$, $M_1 = 0.46 M_{\odot}$, $M_{2,\min} = 0.55 M_{\odot}$ (Brown et al. 2013) (10) HE0320-1917: $P = 0.86492 \text{ d}$, $M_1 = 0.29 M_{\odot}$, $M_{2,\min} = 0.35 M_{\odot}$ (Nelemans et al. 2005) (11) WD0032-317: possible 1500 K BD companion, based on weak NIR excess. (12) WD1013-010: $P = 0.43653 \text{ d}$, $M_1 = 0.44 M_{\odot}$, $M_{2,\min} = 0.38 M_{\odot}$ (Nelemans et al. 2005) (13) HE0516-1804: possible NIR excess indicating a $T_{\text{eff}} \sim 3000 \text{ K}$ companion with radius $\sim 0.2 R_{\odot}$.

unreliable, and this could also lead to the appearance of a too-red NIR spectral slope. In the third case, WD0032-317, a small excess seen at 3.35 and $4.6 \mu\text{m}$ may in fact be from a BD companion. Finally, the fourth case with a NIR excess is HE0516-1804, where we find factor-2 discrepancies between different optical photometric measurements, but the NIR photometry nonetheless suggests the

presence of a strong excess, corresponding to a $\sim 3000 \text{ K}$, $0.2 R_{\odot}$ -radius emitter (such as an M4-M5 dwarf companion). The red part of the SPY spectrum is smooth, with no traces of any stellar absorption features that we would expect given such a stellar companion, but this may be expected for a companion as cool as this (see above). The nature of the companion in this case is therefore

still unclear, and deserves further study. Among the 43 tail WDs, there may thus be one or two WDs whose RV variations are caused by an M star or by a ~ 1500 K BD companion.

From a statistical point of view, dedicated studies using NIR excess to discover unresolved BD companions in WD samples have estimated a WD+BD binary fraction of 0.5 ± 0.3 per cent (Steele et al. 2011), and 0.8 to 2 per cent (Girven et al. 2011). Thus, in the full SPY sample analysed here, one might expect a handful of WD+BD binaries at all separations out to thousands of AU. Assuming roughly equal numbers per logarithmic interval of separation, about 1/3 of those systems would be in the < 4 AU separation range probed by the tail WDs, i.e. one or two systems. This is consistent with our NIR-excess search results, above, for the tail WDs. In summary, the maximum contamination of WD+BD and WD+dM systems to the ΔRV_{\max} tail population is by one or two systems, and the overwhelming majority of the rest must be WDs with compact-remnant companions. Many binaries are known consisting of a WD plus a neutron star (see Lorimer 2001), and systems of a WD plus a black hole also likely exist. However, such systems are expected to be ~ 100 times rarer than DWDs (e.g. Nelemans et al. 2001) so it is unlikely that they are in our sample, let alone in significant numbers. We will therefore assume from here on that the tail of the ΔRV_{\max} distribution probes primarily the DWD population.

As an aside, among the 19 DAZ WDs with a photospheric Ca II K ($\lambda 3933.7 \text{ \AA}$) absorption line (Koester et al. 2005) that have multiple epochs, we tested for any changes in the equivalent width of the lines between epochs. The time differences span the full range of the sample – some are a few days, some a few weeks, and some several months to a year. Photospheric metal absorption in WDs results from recent or ongoing accretion of planetary debris (e.g. Jura 2003; Koester et al. 2014), and it is not unreasonable to expect that the WD photospheric abundances could change on these timescales due to changes in accretion rate and gravitational settling of the accreted ions. However, we detect no changes in Ca II K equivalent width in any of these WDs, to $\lesssim 0.03 \text{ \AA}$.

3 MONTE CARLO SIMULATION OF THE ΔRV_{\max} DISTRIBUTION OF THE BINARY WD POPULATION OBSERVED BY SPY

To use the observed ΔRV_{\max} distribution to set constraints on the DWD population, we now simulate families of assumed binary WD populations. We then “observe” each simulated population with the sampling sequences and the velocity error distributions of the real data, to produce a model ΔRV_{\max} distribution for each simulated population. Except for a number of minor updates, our methodology follows closely the one in M12 and BM12. For convenience, we re-describe it here briefly.

As noted in M12, our modelling approach is distinct from that of “binary population synthesis” (BPS) calculations (Ruiter et al. (e.g. 2009); Mennekens et al. (e.g. 2010); Toonen et al. (e.g. 2011)). In BPS, one simulates the evolution of a population of main-sequence binaries, from its initial mass and separation distributions, through the various stages of stellar and binary evolution, including mass transfer, mass loss, and common envelope. Due to the multiplicity of free parameters for the initial conditions, and the highly simplified treatment of the physical processes, there is large variety in the predictions of different BPS models. Here, in contrast, we parametrise the properties of the DWD population only at end of last common-envelope phase, after which gravitational wave emission alone drives the decay of the orbit. By skipping over the pre-

vious phases of evolution, our approach permits testing regions of the parameter space describing the true DWD population that may not be accessible to BPS, because no calculated BPS models have led to those regions.

To simulate a WD system (single or binary) we first assign it a primary mass, m_1 (‘primary’ and ‘secondary’ refers here to the larger and smaller mass, respectively, not the photometric property). The primary mass is drawn from the observed WD mass function found by Kepler et al. (2015) for 1504 hot (effective temperature $T_{\text{eff}} > 12000$ K) DA WDs with $S/N > 10$ in the DR10 SDSS catalogue. We use the Kepler et al. (2015) representation of the WD mass distribution with three Gaussian components – a main, narrow, component centred at $0.65 M_{\odot}$, with 1σ width of $0.044 M_{\odot}$, a second component centred at $0.57 M_{\odot}$, of width $0.097 M_{\odot}$, and height 0.17 of the main component, and a third component centred at $0.81 M_{\odot}$, of width $0.187 M_{\odot}$, and height 0.06 of the main component. Compared with the WD mass function of Kepler et al. (2007), used in M12 and BM12, this updated WD mass function is mildly changed: its peak is at slightly higher masses, by about $0.05 M_{\odot}$, it has a more prominent component of $\gtrsim 0.9 M_{\odot}$ WDs, and it has a less prominent component of $\lesssim 0.4 M_{\odot}$ WDs. We find that only the low-mass component in the Kepler et al. (2007) mass distribution changes the calculated model ΔRV_{\max} distributions and, if used, it mainly shifts the allowed range of model values of the binarity fraction f_{bin} , up by ~ 0.02 . However, the primaries in DWDs likely have a mass distribution distinct from that of single WDs, particularly in close DWDs that have been affected by mass transfer and mass loss. We further study in Section 4 the effect of the assumed primary mass distribution on our conclusions.

Our final sample’s RV precision and the time intervals between epochs bound the range of WD separations within which RV changes can indicate binarity and hence within which the binary fraction f_{bin} can be constrained. In an extreme-mass-ratio WD binary with masses $m_1 = 1.2 M_{\odot}$ and $m_2 = 0.2 M_{\odot}$ and separation a , the secondary (m_2) will have circular velocity and period

$$v_{\text{circ}} = 30 \text{ km s}^{-1} (a/\text{AU})^{-1/2}, \quad P = 308 \text{ d} (a/\text{AU})^{3/2}, \quad (1)$$

respectively. If the system is optimally inclined to our line of sight ($i = 90^\circ$), and it is observed at the two quadrature phases, i.e. with an epoch separation $\Delta t = P/2$, yielding an RV velocity difference between epochs of $\Delta RV = 2v_{\text{circ}}$, then

$$\frac{\Delta RV}{\Delta t} = \frac{4 \times 30 \text{ km s}^{-1}}{308 \text{ d}} \left(\frac{a}{\text{AU}} \right)^{-2}. \quad (2)$$

Thus, the largest-separation DWD systems to which the sample is sensitive have

$$a = 1 \text{ AU} \left(\frac{\Delta RV}{120 \text{ km s}^{-1}} \right)^{-1/2} \left(\frac{\Delta t}{308 \text{ d}} \right)^{1/2}. \quad (3)$$

Our sample, with a minimum detectable $\Delta RV \approx 10 \text{ km s}^{-1}$ and maximum separation between epochs of $\Delta t = 470 \text{ d}$, is thus sensitive to DWD systems with separations out to $a \approx 4 \text{ AU}$. We therefore define f_{bin} as the fraction of all WD systems (both single systems and binary systems) that are binary systems with separations $a < 4 \text{ AU}$.

WDs with masses less than $m_{\text{lim}} \approx 0.45 M_{\odot}$ cannot form in isolation over a Hubble time, and therefore must have been in close-separation binaries such that interactions affected the stellar evolution of the WD progenitors. Indeed, ELM WDs with masses $< 0.25 M_{\odot}$ are always observed to be in binaries (Brown et al. 2016). Nonetheless, 30 per cent of WDs with masses $0.32 M_{\odot} < M < 0.45 M_{\odot}$ may be single after all (Brown et al. 2011), with a

number of mechanisms having been proposed for this singularity (see [Brown et al. 2011](#); [Zorotovic & Schreiber 2016](#)). We account for these observations by assigning binary companions to 70% of the simulated WD primaries in the $0.25 - 0.45 M_{\odot}$ mass range. (In this we differ from the treatment in [BM12](#), where WDs in this mass range had a probability f_{bin} for binarity.) Simulated primary WDs with mass $< m_{\text{lim}} = 0.25 M_{\odot}$, are always assigned to binaries. The fraction of the [Kepler et al. \(2015\)](#) mass function that is either below $m_{\text{lim}} = 0.25 M_{\odot}$, 0.025%, or between $0.25 M_{\odot}$ and $0.45 M_{\odot}$, 2.7%, means that 0.025% of the simulated WDs in the sample are in binaries with one of the WDs having $< 0.25 M_{\odot}$, $0.7 \times 2.7\% = 1.9\%$ are binaries with one WD in the $0.25 - 0.45 M_{\odot}$ range, and a fraction $f_{\text{bin}} - (0.00025 + 0.7 \times 0.027)$ of simulated WDs are in binary systems in which both components have masses above $m_{\text{lim}} = 0.45 M_{\odot}$.

To the simulated WDs chosen to be in binaries, additional binary parameters are assigned, as we will describe below. To the remaining $1 - f_{\text{bin}}$ fraction of the WDs are given an orbital velocity of zero, and the simulation goes directly (see below) to the allocation of random velocity errors at several observing epochs.

Following [M12](#), we draw the secondary WD mass, m_2 , from a power-law distribution in mass ratio,

$$P(q) \propto q^{\beta}, \quad q \equiv m_2/m_1, \quad (4)$$

with m_2 between $0.45 M_{\odot}$ and m_1 . The parameter β can be zero (equal probability for all mass ratios in the range), positive (preference for similar-mass DWDs), or negative (preference for low-mass companions). The power-law index β is one of the parameters of the WD binary population that could, in principle, be constrained by the data, but in practice we find that the ΔRV_{max} distribution is only weakly sensitive to it (as shown also in [BM12](#) for the SDSS WD dataset). In cases where the primary in the Monte-Carlo draw was below $0.25 M_{\odot}$ (and hence the WD is always in a binary), or the primary is in the $0.25 M_{\odot}$ to $0.45 M_{\odot}$ range (and hence it has a 70% probability of being in a binary), then m_2 is chosen with equal probability between $0.2 M_{\odot}$ and $1.2 M_{\odot}$.

We assume in our simulations an initial power-law WD separation distribution at the end of the final common-envelope phase, with an index α that is to be constrained by the observations. Apart from the physical and observational arguments for such a functional form (see [M12](#) and [BM12](#)), the range of separations that we consider here, $\sim 0.001 - 4$ AU, is limited enough that a power-law can approximate a broad range of other, monotonic, functional dependences. Orbital decay due to gravitational wave emission will modify any initial separation distribution with time, as all of the orbits shrink, and the tightest systems merge. The distribution at a given time will be the integral over populations of different ages. [M12](#) calculated analytic expressions for this evolved, time-integrated, distribution of DWD separations, under some simplifying assumptions, and we briefly repeat here the salient points.

The separation a between two point masses, m_1 and m_2 , in a circular orbit shrinks over time due to gravitational-wave losses as

$$\frac{da}{dt} = -\frac{K}{4a^3}, \quad K \equiv \frac{256}{5} \frac{G^3}{c^5} m_1 m_2 (m_1 + m_2). \quad (5)$$

The time t to evolve from separation a' to separation a follows

$$a'^4 - a^4 = Kt. \quad (6)$$

Assume that a co-eval population of WD binaries forms at a time $t = 0$, after having emerged from their final common envelope phase, with an initial distribution of separations $n'(a')$, assumed

independent of separation. For the evolved distribution $n(a, t)$, conservation of the number of systems,

$$n(a, t) da = n'(a') da', \quad (7)$$

and assuming the initial distribution is a power law,

$$n'(a') \propto a'^{\alpha}, \quad (8)$$

then gives

$$n(a, t) \propto a^3 (a^4 + Kt)^{(\alpha-3)/4}, \quad (9)$$

a broken power law. At separations $a \gg (Kt)^{1/4}$ (i.e., much larger than those that can merge within time t), the distribution has the original power-law slope, $n(a) \sim a^{\alpha}$. For $a \ll (Kt)^{1/4}$, $n(a) \sim a^3$ (see figure 3 of [M12](#)).

Assuming a series of binary WD generations, produced at a constant rate between $t = 0$ and the current age of the Galaxy, t_0 , the present separation distribution is

$$N(x) \propto x^{4+\alpha} [(1+x^{-4})^{(\alpha+1)/4} - 1], \quad \alpha \neq -1, \quad (10)$$

or

$$N(x) \propto x^3 \ln(1+x^{-4}), \quad \alpha = -1, \quad (11)$$

where

$$x \equiv \frac{a}{(Kt_0)^{1/4}} \quad (12)$$

is the separation scaled to that of binaries that merge within the Galaxy lifetime. For example, for $t_0 = 13.6$ Gyr and $m_1 = m_2 = 0.6 M_{\odot}$, $x = 1$ corresponds to $a_0 \approx 2.5 R_{\odot}$. $N(x)$ is, again, roughly a broken power law, with index α at $x \gg 1$. At $x \ll 1$ the power-law index is 3 for $\alpha \geq -1$, and $\alpha + 4$ for $\alpha \leq -1$. Even if the star-formation history is ‘‘bumpy’’ rather than constant, as assumed above, the WD formation history will be the convolution of the star-formation history with a broad, $\sim t^{-0.5}$, kernel, that describes the WD supply rate from a coeval single stellar population, which will smooth out the WD production rate. Therefore Eqns. 10–11 hold, as long as the star-formation history falls less steeply than $\sim t^{-0.5}$.

In every realization of our simulations, we draw each simulated DWD separation from the distributions described by Eqns. 10–11 for a particular value of α , with a between $a_{\text{min}} = 2 \times 10^4$ km (DWD contact) and $a_{\text{max}} = 4$ AU. For each simulated DWD system, Kepler’s law gives the period

$$\tau = 2\pi \left(\frac{a^3}{G(m_1 + m_2)} \right)^{1/2}, \quad (13)$$

and the (assumed circular) orbital velocities,

$$v_1 = \frac{2\pi a}{\tau} \frac{m_2}{m_1 + m_2}, \quad v_2 = \frac{2\pi a}{\tau} \frac{m_1}{m_1 + m_2}. \quad (14)$$

Binaries with periods < 10 min are assigned zero orbital velocity, as the exposure times of the individual VLT spectra prevent detection of velocity differences in such cases.

The merger rate per WD, for a given set of parameters, is obtained numerically by counting the fraction of all of the systems in the simulation whose merger lifetime, $t_{\text{merge}} = a^4/K$ (Eq. 6 with $a = 0$) is smaller than some time interval, divided by that time interval. Recent observational estimates of the Milky Way’s disk space density of WDs are all broadly consistent and include $0.0046 \pm 0.0005 \text{ pc}^{-3}$, from a proper-motion selected sample of WDs in SDSS ([Harris et al. 2006](#)), $0.0049 \pm 0.0005 \text{ pc}^{-3}$ for a sample within 20 pc ([Sion et al. 2009](#)), $0.0048 \pm 0.0005 \text{ pc}^{-3}$ for a sample within 25 pc ([Holberg et al. 2016](#)), and $0.0055 \pm 0.0001 \text{ pc}^{-3}$ using

a large new proper motion catalogue of SDSS WDs (Munn et al. 2016). The local stellar mass density is $0.085 M_{\odot} \text{pc}^{-3}$ (McMillan 2011). Dividing it by the WD space density of Munn et al. (2016), there are $15.5 M_{\odot}$ of stellar mass in the disk per WD. We therefore divide the DWD merger rate per WD by $15.5 M_{\odot}$ to convert it to a DWD merger rate per unit stellar mass. Adopting the slightly lower value of Holberg et al. (2016) for the WD density would systematically lower all of our model merger rates by 15 per cent.

A line-of-sight inclination i angle of the the orbital plane is chosen for each system and the line-of-sight velocity is reduced by $\sin i$. The photometric primary WD, which determines which of the two WD’s RVs is measured, can be either the less or more massive WD, depending on the WD surface areas (dictated mainly by mass) and temperatures (set by cooling age, and potentially complicated by interactions between the binary components). Following the observational and theoretical considerations in M12, we make the less massive WD the photometric primary when its mass is below $0.35 M_{\odot}$, but decide randomly, with equal probability, between the two WDs when the less massive WD is above this limit. We have tested the sensitivity of the results to this assumption by trying *always* to take the lower-mass WD as the photometric primary. We find negligible changes.

The line-of-sight velocity (i.e. RV) curve of the photometric primary is sampled with the actual distribution of temporal samplings in our SPY sample, by applying at random a particular real observation pattern (number of epochs and time between epochs) from the sample. Every simulated velocity measurement is noised with a random error, drawn from a Gaussian distribution. The variance of the Gaussian, in turn, is drawn from the distribution of measurement errors of the observed sample (see Figure 2). Finally, to calculate ΔRV_{\max} , we find the difference between the minimum and maximum observed velocities for every simulated DWD or single WD. We create 4×10^5 WD systems (some single, some binary, according to f_{bin}) for every parameter combination that defines a DWD population model. The fractional prediction for each bin in the model ΔRV_{\max} distribution, multiplied by the observed WD sample size, gives the expectation value for that bin.

M12 discussed how, for the SDSS sample, the ΔRV_{\max} distribution depends on the binary population parameters f_{bin} , α , and β . We show this in Figure 3 for the SPY sample, with its much higher RV resolution, which probes DWDs at larger separations and smaller orbital velocities. The ΔRV_{\max} distribution strongly discriminates in f_{bin} , which affects the amplitude in the $\sim 10 - 100 \text{ km s}^{-1}$ range. Changes in α affect the slope of the distribution in the range, but a larger relative range is consistent with the observations, and only more extreme values of α are excluded. As already noted, the ΔRV_{\max} distribution depends weakly on β , the power-law index of the binary mass-ratio distribution, so RV survey data of the type considered here do not constrain this binary population characteristic. Conversely, not knowing the distribution of mass ratios does not affect adversely our ability to constrain the other binary population parameters.

To compare each simulated model ΔRV_{\max} distribution to the observed one, we take the model expectation value for each velocity bin in the ΔRV_{\max} distribution, and we sum the logarithms of the Poisson probabilities of finding the observed number of systems in each bin, given the expectations from the model. This gives the log of the likelihood of each model. We run models over a grid in parameter space, to find the allowed region of the DWD population parameter space.

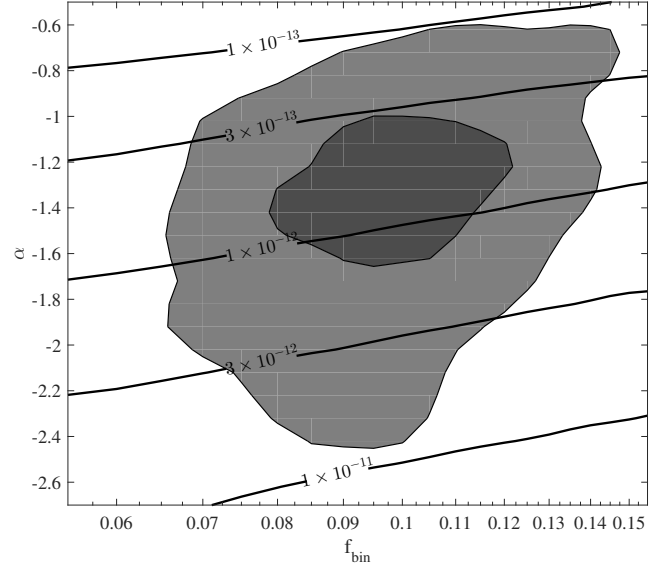


Figure 4. Likelihood contours in the f_{bin}, α plane, indicating the 1σ (dark gray) and 2σ (light gray) confidence levels. The overlaid lines are curves of constant WD merger rate in $\text{yr}^{-1} M_{\odot}^{-1}$, as marked. The Milky Way’s specific SN Ia rate is $R_{\text{Ia}} \approx 1.1 \times 10^{-13} \text{ yr}^{-1} M_{\odot}^{-1}$

4 RESULTS

Figure 4 shows the parameter space of f_{bin} and α , with contours showing the 1σ and 2σ likelihood ranges, corresponding to changes of 0.5 and 2, respectively, in log-likelihood compared to the best-fit model. Models acceptable at the 2σ level occupy a well-defined region in the $f_{\text{bin}}-\alpha$ plane, with f_{bin} going from ~ 0.07 to 0.14 as α goes from -2.4 to -0.6 . The best-fit 1σ ranges are $f_{\text{bin}} = 0.100 \pm 0.020$ and $\alpha = -1.32 \pm 0.30$. These constraints are significantly improved compared to those from the SDSS WD sample in BM12. Also shown in Figure 4 are curves of constant merger rate, which in this kind of presentation (linear in α , logarithmic in f_{bin}) appear roughly as straight lines (see M12). The acceptable models (over the 2σ region) span merger rates of $R_{\text{merge}} = 1 \times 10^{-13} \text{ yr}^{-1} M_{\odot}^{-1}$ to $8 \times 10^{-12} \text{ yr}^{-1} M_{\odot}^{-1}$. The likelihood-weighted merger rate over the 1σ region is $(7 \pm 2) \times 10^{-13} \text{ yr}^{-1} M_{\odot}^{-1}$.

The observed ΔRV_{\max} distribution (Figure 3) identifies 43 systems that are candidate DWDs in the distribution’s “tail” (i.e. beyond the “core” of the distribution that is produced by RV errors in single WDs, and by the DWDs that are not fortuitously time-sampled or insufficiently inclined to the line of sight). See Table 1 for the full candidate list. 27 of them are very likely DWD systems (with $\Delta RV_{\max} > 15 \text{ km s}^{-1}$) and a further 16 (with $10 \text{ km s}^{-1} < \Delta RV_{\max} < 15 \text{ km s}^{-1}$) are possible DWDs. Among the 43, 13 cases are double-lined DWDs. Koester et al. (2009) have derived and compiled T_{eff} and log surface gravity ($\log g$) estimates for the SPY WDs from modelling of the WD absorption line profiles with synthetically calculated WD atmosphere spectra. They note that the atmospheric fits assumed a single WD, and hence the results for the double-lined systems are approximate. As described in Section 2, we corrected for 3D effects using Tremblay et al. (2013), and used the theoretical WD cooling sequences of Fontaine et al. (2001) to derive masses for all of the WDs. We list them in Tables 1 and A1.

Figure 5 compares the mass distributions of the photometric-primary WDs in our full SPY sample and for the likely DWD systems (from the “tail” of the ΔRV_{\max} distribution). The mass dis-

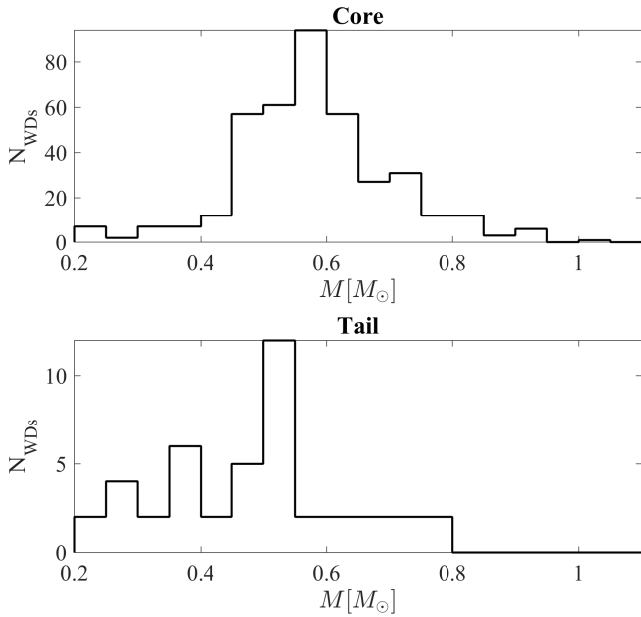


Figure 5. Estimated mass distributions of the mostly single WDs from the “core” of the ΔRV_{\max} distribution (top panel) and of the visible photometric primaries among the DWDs from the ΔRV_{\max} distribution’s $> 10 \text{ km s}^{-1}$ “tail” (bottom panel).

tribution of the SPY WDs is quite similar to that of Kepler et al. (2007) for SDSS WDs in the sense of having a significant low-mass WD component. The photometric primaries among the SPY DWD candidates, however, are clearly biased to lower masses. This is not surprising, since most or all of these systems must have undergone common-envelope evolution, which can stunt the growth of the degenerate core of the evolved star in the system, and thus produce WDs below the $\sim 0.45 M_{\odot}$ Hubble-time stellar-evolution limit.

The question naturally arises as to the masses of the unseen photometric secondary WDs in the DWD systems. Unfortunately, the SPY few-epoch observations cannot answer this question. More intensive RV measurements exist for 14 of these systems (Saffer et al. 1988; Bergeron et al. 1989; Marsh et al. 1995; Napiwotzki et al. 2002; Karl et al. 2003a,b; Nelemans et al. 2005; Morales-Rueda et al. 2005; Brown et al. 2013). There is some indication that the companion masses, also listed for these cases in Tables 1 and A1, tend to be similar to, or slightly larger than, those of the photo-primary WDs, but the number is still too small for a clear picture of the photo-secondary mass distribution. However, it is interesting to note that for the sample of 62 ELM $\sim 0.2 M_{\odot}$ WDs of Brown et al. (2016), the unseen photo-secondary WDs have a broad mass distribution with a mean mass about four times higher than the ELMs, with a significant fraction of companion WDs at masses $> 0.9 M_{\odot}$. It is at-least conceivable that a similar trend exists for the DWD systems in SPY, with the relatively low-mass photometric-primary WDs accompanied, in many cases, by $> 0.9 M_{\odot}$ or $> 1.0 M_{\odot}$ WDs. Recent “violent merger” hydrodynamical simulations of DWD mergers (Pakmor et al. 2012; Ruitter et al. 2013; Pakmor et al. 2013) suggest that if one of the merging WDs is above such a mass, an off-center ignition can be set off in the accretion flow onto that WD, and can in turn set off a detonation wave through its high-density interior, producing an explosion that agrees with observed SN Ia properties. If the true DWD merger rate is sufficiently in the high end of the allowed range in Figure 4, Section 3, when we experimented with replacing the Kepler et al.

(2015) plus a large-enough fraction of DWDs have a massive WD binary component, and the violent-merger mechanism works, then some or even all SN Ia events would be explainable as DWD mergers.

To test whether the type of mass distributions for the DWD components just discussed are still consistent with the observed SPY ΔRV_{\max} distribution and the allowed region of $f_{\text{bin}}-\alpha$ parameter space that we have delineated, we have run several more simulation grids of models. Instead of choosing the mass-primary WD from the Kepler et al. (2015) WD mass function, we chose the mass primary from a three-Gaussian fit to the actual mass distribution of the SPY photo-primaries in Figure 5 (top panel). The Gaussian components are a main component centred at $0.55 M_{\odot}$, with 1σ width of $0.07 M_{\odot}$, a second component centred at $0.72 M_{\odot}$, of width $0.1 M_{\odot}$, and height 0.24 of the main component, and a third component centred at $0.3 M_{\odot}$, of width $0.078 M_{\odot}$, and height 0.10 of the main component. The secondary mass selection and the rest of the simulation procedure remain as before. We find that, with this SPY-sample mass distribution, the allowed regions in $f_{\text{bin}}-\alpha$ parameter space change slightly: the f_{bin} values of the allowed regions are shifted up by ≈ 0.02 , while 1σ region expands to include also α values that are more negative by ~ -0.2 . (This trend is not surprising since, as noted above, the SPY WD mass distribution somewhat resembles that of Kepler et al. (2007), and as described in Section 3, when we experimented with replacing the Kepler et al. (2015) mass function with the Kepler et al. (2007) mass function, we obtained a similar shift.)

As a further test of the systematic dependence of our results on the assumed simulated DWD masses, we have repeated the experiment, but now drawing the *photo*-primary of every simulated DWD from a 3-Gaussian fit to the observed mass distribution of the 43 DWD candidates from the tail of the ΔRV_{\max} distribution (Figure 5, bottom panel). Here, the Gaussian components are a main component centred at $0.51 M_{\odot}$, with 1σ width of $0.024 M_{\odot}$, a second component centred at $0.35 M_{\odot}$, of width $0.087 M_{\odot}$, and height 0.35 of the main component, and a third component centred at $0.68 M_{\odot}$, of width $0.1 M_{\odot}$, and height 0.18 of the main component. The unseen second WD was chosen from a broad Gaussian centred at $0.75 M_{\odot}$, with $\sigma = 0.25 M_{\odot}$, similar to the one deduced by Brown et al. (2016) for the mass distribution of the ELM WD companions. Compared to the results in Figure 4, Section 3, where we assumed the Kepler et al. (2015) mass function, with these choices the allowed contours shift vertically up in α by ~ 0.2 . Considering the model uncertainty in the distributions of the DWD masses, as explored by this range of experiments, we adopt *systematic* uncertainties $+0.02$ in f_{bin} and ± 0.2 in α , compounding the random uncertainties, discussed previously.

5 CONCLUSIONS

We have measured and analysed the distribution of maximum radial velocity differences between observing epochs, ΔRV_{\max} , for a sample of 439 DA-type WDs from the SPY program, and have modelled the ΔRV_{\max} distribution to set constraints on the properties of the DWD population. Assuming that every generation of the DWD population, when it emerges from its last common-envelope phase, has an initial separation distribution that can be represented by a power law over the $a < 4 \text{ AU}$ separation range probed by these data, then the fraction of all WDs that have companion WDs in this separation range is $f_{\text{bin}} = 0.10 \pm 0.020(1\sigma) + 0.02$ (systematic), and the power-law index of the separation distri-

bution is $\alpha = -1.3 \pm 0.30(1\sigma) \pm 0.2$ (systematic). Combined with current estimates of the local WD space density and the local stellar mass density, these parameters imply a gravitational-wave-loss-driven specific Milky Way WD merger rate of 1×10^{-13} to $8 \times 10^{-12} \text{ yr}^{-1} M_{\odot}^{-1}$ (2σ range). This is between 1 to 70 times the estimated Milky-Way SN Ia rate per unit mass. If some fraction (perhaps as small as a few per cent) of DWD mergers can produce a normal SN Ia explosion, our results imply that there is no shortage of the progenitor DWD population for this explosion scenario.

Our results indicate about a 3% DWD binary fraction per decade in separation among WDs. Klein & Katz (2017) have recently estimated the binary fraction among DWD stellar progenitors, where both progenitors have $> 1 M_{\odot}$, and found a 4% fraction per decade in period, corresponding to 6% per decade in separation, with some overlap between the separation ranges probed by their analysis and ours. In a Galactic population of WDs in binaries, for roughly half of the systems with WD companions having initial mass $> 1 M_{\odot}$, the companions will not yet have evolved into a WD, and therefore the companions will completely dominate the light, preventing the inclusion of such systems in WD samples. The 3% fraction of DWDs per decade in separation that we see in SPY is therefore nicely consistent with the 6% per decade found by Klein & Katz (2017) for DWD progenitors.

The high- ΔRV_{max} tail of the distribution identifies 27 very likely DWD systems (with $\Delta RV_{\text{max}} > 15 \text{ km s}^{-1}$; in two cases the WD companions may be a BD and a cool M star) and a further 16 possible DWD systems (with $10 \text{ km s}^{-1} < \Delta RV_{\text{max}} < 15 \text{ km s}^{-1}$). The ΔRV_{max} distribution does not constrain the component masses of the DWDs, and thus these DWDs merit follow-up observations to confirm their nature and to derive their orbital parameters and component masses. From photospheric modelling, the masses of the photometric primaries in the DWDs tend to be of somewhat lower mass than typical single WDs, with a broad distribution centred around $\sim 0.5 M_{\odot}$. The minority of these DWDs that have additional data in the literature generally have, for the unseen photo-secondary WDs, masses similar to, or somewhat larger than, the photo-primary.

The “double-degenerate” scenario for SNe Ia, invoking DWD mergers as the progenitors of SNe Ia, has been traditionally criticised on two main grounds (see Maoz et al. 2014). The numbers and hence the merger rate of the progenitor DWD populations was thought to be too small to match the SN Ia rate, particularly if a total merged mass above the Chandrasekhar mass is required for an explosion, as often assumed in this scenario. The second long-standing problem has been theoretical – the tidal disruption of the secondary-mass WD by the primary, and its gradual accretion onto the primary WD through a disk or a spherical configuration was thought to lead to either a stable, just more-massive, merged WD or, in the case of an above-Chandrasekhar final mass, to an “accretion-induced collapse” to a neutron star and an electron-capture supernova explosion. (However, the accretion-induced collapse outcome has emerged from one-dimensional calculations, which could change in 3D treatments, that are yet to be performed.)

Our results for the DWD population are germane to both of these objections to the double-degenerate SN Ia scenario. It is possible that follow-up observations of the SPY DWDs will reveal, in analogy to what has been found for ELM WDs, that their WD companions have a broad mass distribution, with a significant fraction at masses above 0.9 or $1 M_{\odot}$. If so, and given that our results allow for up to a factor-70 surplus in the total rate of DWD mergers, there could conceivably be a sufficient number of mergers of CO+CO WDs with above-Chandrasekhar merged masses. Alterna-

tively, recent violent-merger models (e.g. Pakmor et al. 2012) find that an above-Chandrasekhar total mass is not required for reproducing a normal SN Ia explosion, but rather only a primary mass above 0.9 or $1 M_{\odot}$. The secondary, which could even be a low-mass He WD, serves only as a “hammer” that sets off the detonation in the primary. If this were true, then an even-larger fraction of the total DWD merger rate could lead to a SN Ia explosion. A remaining problem for violent mergers is the asymmetry of the explosion predicted by current models, and manifested in the expected strong (but unobserved in practice) polarisation of the light from SNe Ia (Bulla et al. 2016).

On the observational side, progress is achievable from follow-up observations and detailed characterisation of the individual DWD systems. Upcoming large and complete WD and DWD samples from the *Gaia* Mission will bring into much better focus the DWD population and its merger rate. In parallel, continued improvements in the theoretical study of WD mergers should further clarify if and under what conditions mergers can lead to SN Ia explosions.

ACKNOWLEDGEMENTS

We thank the original SPY survey team for their efforts in proposing and obtaining this valuable observational dataset. We are grateful to Carles Badenes, Ira Bar, Uri Malamud (who suggested the Ca II K equivalent width test), and Yossi Shvartzvald for their contributions to this work. The anonymous referee is thanked for constructive criticisms that improved this paper. This work was supported by Grant 648/12 by the Israel Science Foundation (ISF) and by Grant 1829/12 of the I-CORE program of the PBC and the ISF. We acknowledge the hospitality of the Munich Institute for Astro- and Particle Physics, where this work was completed. Based on data obtained from the ESO Science Archive Facility for programmes 165.H-0588 and 167.D-0407. This research has made use of the VizieR catalogue access tool, CDS, Strasbourg, France. This publication makes use of data products from the Two Micron All Sky Survey, which is a joint project of the University of Massachusetts and the Infrared Processing and Analysis Center/California Institute of Technology, funded by the National Aeronautics and Space Administration and the National Science Foundation. This publication makes use of data products from the Wide-field Infrared Survey Explorer, which is a joint project of the University of California, Los Angeles, and the Jet Propulsion Laboratory/California Institute of Technology, funded by the National Aeronautics and Space Administration.

REFERENCES

- Badenes C., Maoz D., 2012, *ApJ*, **749**, L11
- Baraffe I., Chabrier G., 1996, *ApJ*, **461**, L51
- Bergeron P., Wesemael F., Fontaine G., Liebert J., 1989, *ApJ*, **345**, L91
- Brown J. M., Kilic M., Brown W. R., Kenyon S. J., 2011, *ApJ*, **730**, 67
- Brown W. R., Kilic M., Allende Prieto C., Gianninas A., Kenyon S. J., 2013, *ApJ*, **769**, 66
- Brown W. R., Gianninas A., Kilic M., Kenyon S. J., Allende Prieto C., 2016, *ApJ*, **818**, 155
- Bulla M., Sim S. A., Pakmor R., Kromer M., Taubenberger S., Röppe F. K., Hillebrandt W., Seitenzahl I. R., 2016, *MNRAS*, **455**, 1060
- Christlieb N., Wisotzki L., Reimers D., Homeier D., Koester D., Heber U., 2001, *A&A*, **366**, 898
- Cutri R. M., et al. 2014, VizieR Online Data Catalog, **2328**

- Debes J. H., Kilic M., Tremblay P.-E., López-Morales M., Anglada-Escude G., Napiwotzki R., Osip D., Weinberger A., 2015, *AJ*, **149**, 176
- Demers S., Wesemael F., Irwin M. J., Fontaine G., Lamontagne R., Kepler S. O., Holberg J. B., 1990, *ApJ*, **351**, 271
- Duquenois A., Mayor M., 1991, *A&A*, **248**, 485
- Edge A., Sutherland W., Kuijken K., Driver S., McMahon R., Eales S., Emerson J. P., 2013, *The Messenger*, **154**, 32
- Falcon R. E., Winget D. E., Montgomery M. H., Williams K. A., 2010, *ApJ*, **712**, 585
- Fontaine G., Brassard P., Bergeron P., 2001, *PASP*, **113**, 409
- Girven J., Gänsicke B. T., Steeghs D., Koester D., 2011, *MNRAS*, **417**, 1210
- Hagen H.-J., Groote D., Engels D., Reimers D., 1995, *A&AS*, **111**, 195
- Hallakoun N., et al., 2016, *MNRAS*, **458**, 845
- Harris H. C., et al., 2006, *AJ*, **131**, 571
- Holberg J. B., Oswalt T. D., Sion E. M., McCook G. P., 2016, *MNRAS*, **462**, 2295
- Jarvis M. J., et al., 2013, *MNRAS*, **428**, 1281
- Jura M., 2003, *ApJ*, **584**, L91
- Karl C., Napiwotzki R., Heber U., Lisker T., Nelemans G., Christlieb N., Reimers D., 2003a, in de Martino D., Silvotti R., Solheim J.-E., Kalytis R., eds. Vol. 105, NATO ASIB Proc. 105: White Dwarfs. p. 43 ([arXiv:astro-ph/0210004](https://arxiv.org/abs/astro-ph/0210004))
- Karl C. A., Napiwotzki R., Nelemans G., Christlieb N., Koester D., Heber U., Reimers D., 2003b, *A&A*, **410**, 663
- Kepler S. O., Kleinman S. J., Nitta A., Koester D., Castanheira B. G., Giovannini O., Costa A. F. M., Althaus L., 2007, *MNRAS*, **375**, 1315
- Kepler S. O., et al., 2015, *MNRAS*, **446**, 4078
- Kilkenny D., O'Donoghue D., Stobie R. S., 1991, *MNRAS*, **248**, 664
- Klein Y. Y., Katz B., 2017, *MNRAS*, **465**, L44
- Koester D., Rollenhagen K., Napiwotzki R., Voss B., Christlieb N., Homeier D., Reimers D., 2005, *A&A*, **432**, 1025
- Koester D., Voss B., Napiwotzki R., Christlieb N., Homeier D., Lisker T., Reimers D., Heber U., 2009, *A&A*, **505**, 441
- Koester D., Gänsicke B. T., Farihi J., 2014, *A&A*, **566**, A34
- Lamontagne R., Demers S., Wesemael F., Fontaine G., Irwin M. J., 2000, *AJ*, **119**, 241
- Lawrence A., et al., 2007, *MNRAS*, **379**, 1599
- Longland R., Lorén-Aguilar P., José J., García-Berro E., Althaus L. G., Isern J., 2011, *ApJ*, **737**, L34
- Lorimer D. R., 2001, *Living Reviews in Relativity*, **4**, 5
- Maoz D., Badenes C., Bickerton S. J., 2012, *ApJ*, **751**, 143
- Maoz D., Mannucci F., Nelemans G., 2014, *ARA&A*, **52**, 107
- Marsh T. R., 2011, *Classical and Quantum Gravity*, **28**, 094019
- Marsh T. R., Dhillon V. S., Duck S. R., 1995, *MNRAS*, **275**, 828
- Maxted P. F. L., Marsh T. R., 1999, *MNRAS*, **307**, 122
- McCook G. P., Sion E. M., 1999, *ApJS*, **121**, 1
- McMillan P. J., 2011, *MNRAS*, **414**, 2446
- Mennekens N., Vanbeveren D., De Greve J. P., De Donder E., 2010, *A&A*, **515**, A89
- Morales-Rueda L., Marsh T. R., Maxted P. F. L., Nelemans G., Karl C., Napiwotzki R., Moran C. K. J., 2005, *MNRAS*, **359**, 648
- Munn J. A., et al., 2016, preprint, ([arXiv:1611.06275](https://arxiv.org/abs/1611.06275))
- Napiwotzki R., et al., 2001, *Astronomische Nachrichten*, **322**, 411
- Napiwotzki R., et al., 2002, *A&A*, **386**, 957
- Napiwotzki R., et al., 2003, *The Messenger*, **112**, 25
- Napiwotzki R., et al., 2004, in Hilditch R. W., Hensberge H., Pavlovski K., eds. *Astronomical Society of the Pacific Conference Series Vol. 318, Spectroscopically and Spatially Resolving the Components of the Close Binary Stars*. pp 402–410 ([arXiv:astro-ph/0403595](https://arxiv.org/abs/astro-ph/0403595))
- Nelemans G., Yungelson L. R., Portegies Zwart S. F., 2001, *A&A*, **375**, 890
- Nelemans G., et al., 2005, *A&A*, **440**, 1087
- Ochsenbein F., Bauer P., Marcout J., 2000, *A&AS*, **143**, 23
- Pakmor R., Kromer M., Taubenberger S., Sim S. A., Röpke F. K., Hillebrandt W., 2012, *ApJ*, **747**, L10
- Pakmor R., Kromer M., Taubenberger S., Springel V., 2013, *ApJ*, **770**, L8
- Raghavan D., et al., 2010, *ApJS*, **190**, 1
- Ruiter A. J., Belczynski K., Fryer C., 2009, *ApJ*, **699**, 2026
- Ruiter A. J., et al., 2013, *MNRAS*, **429**, 1425
- Saffer R. A., Liebert J., Olszewski E. W., 1988, *ApJ*, **334**, 947
- Sion E. M., Holberg J. B., Oswalt T. D., McCook G. P., Wasatonic R., 2009, *AJ*, **138**, 1681
- Skrutskie M. F., et al., 2006, *AJ*, **131**, 1163
- Steele P. R., Burleigh M. R., Dobbie P. D., Jameson R. F., Barstow M. A., Satterthwaite R. P., 2011, *MNRAS*, **416**, 2768
- Toonen S., Nelemans G., Portegies Zwart S., 2011, preprint, ([arXiv:1101.2787](https://arxiv.org/abs/1101.2787))
- Tremblay P.-E., Ludwig H.-G., Steffen M., Freytag B., 2013, *A&A*, **559**, A104
- Voss B., Koester D., Napiwotzki R., Christlieb N., Reimers D., 2007, *A&A*, **470**, 1079
- Wisotzki L., Koehler T., Groote D., Reimers D., 1996, *A&AS*, **115**, 227
- Zorotovic M., Schreiber M., 2016, preprint, ([arXiv:1611.07309](https://arxiv.org/abs/1611.07309))

This paper has been typeset from a $\text{\TeX}/\text{\LaTeX}$ file prepared by the author.

Table 1. WD sample.

Name	RA	Dec	Δt [d]	ΔRV_{\max} [km s ⁻¹]	σ [km s ⁻¹]	N_{σ}	M_1 [M _⊙]	Comments
WD2359-324	00:02:32.36	-32:11:50.7	2.1	12.6	3.0	4.2	0.55	
WD0000-186	00:03:11.21	-18:21:57.6	0.9	0.2	1.5	0.2	0.50	
WD0011+000	00:13:39.19	+00:19:23.1	3.0	3.1	1.2	2.6	0.50	
WD0013-241	00:16:12.63	-23:50:06.4	1.0	2.6	1.2	2.2	0.60	
WD0016-258	00:18:44.49	-25:36:42.2	1.0	3.5	1.7	2.1	0.50	
WD0016-220	00:19:28.23	-21:49:04.9	0.9	1.6	0.9	1.7	0.55	
WD0017+061	00:19:40.99	+06:24:06.2	8.1	2.6	2.9	0.9	0.50	
WD0018-339	00:21:12.90	-33:42:27.4	3.0	1.7	1.1	1.5	0.75	
WD0024-556	00:26:41.08	-55:24:44.9	2.0	3.4	1.5	2.2	0.85	
WD0028-474	00:30:47.16	-47:12:36.9	59.8	116.8	1.7	67.1	0.50	1
WD0029-181	00:32:30.33	-17:53:23.3	0.9	1.5	1.5	1.0	0.65	
HE0031-5525	00:33:36.03	-55:08:37.5	222.2	12.2	4.6	2.7	0.45	
HE0032-2744	00:34:37.91	-27:28:20.0	3.0	5.5	2.6	2.1	0.55	
WD0032-317	00:34:49.82	-31:29:54.3	1.0	38.1	3.8	10.1	0.35	11
WD0032-175	00:35:17.47	-17:18:51.1	7.1	1.9	1.2	1.5	0.50	
WD0032-177	00:35:25.20	-17:30:40.4	7.1	4.8	2.2	2.2	0.70	
WD0033+016	00:35:35.93	+01:53:06.5	8.1	4.3	4.0	1.1	0.95	
WD0037-006	00:40:22.94	-00:21:31.1	45.0	128.5	1.1	118.2	0.55	1
HE0043-0318	00:46:18.38	-03:02:00.8	45.0	2.1	1.0	2.1	0.45	
WD0047-524	00:50:03.74	-52:08:17.1	48.9	0.3	0.8	0.4	0.65	
WD0048-544	00:51:08.87	-54:11:21.2	48.9	1.1	2.0	0.6	0.60	
WD0048+202	00:51:11.00	+20:31:22.3	73.9	2.9	2.4	1.2	0.70	
HE0049-0940	00:52:15.30	-09:24:20.3	0.9	0.3	1.0	0.3	0.45	
WD0050-332	00:53:17.43	-32:59:56.8	319.1	6.5	3.4	1.9	0.60	
WD0052-147	00:54:55.86	-14:26:09.1	0.9	0.7	2.0	0.3	0.75	
WD0053-117	00:55:50.33	-11:27:31.3	0.9	0.2	1.0	0.2	0.20	
HE0103-3253	01:05:30.77	-32:37:54.3	10.1	3.3	1.3	2.4	0.60	
WD0103-278	01:05:53.52	-27:36:56.8	3.9	5.5	0.8	6.8	0.50	
WD0106-358	01:08:20.75	-35:34:43.0	4.0	1.6	2.3	0.7	0.60	
HE0106-3253	01:08:36.07	-32:37:43.5	261.2	0.5	1.1	0.4	0.75	
WD0107-192	01:09:33.13	-19:01:19.2	4.0	1.1	2.7	0.4	0.55	
WD0108+143	01:10:55.14	+14:39:21.3	4.0	0.7	3.0	0.2	0.75	
WD0110-139	01:13:09.85	-13:39:35.8	3.0	3.3	2.5	1.3	0.65	
WD0114-605	01:16:19.55	-60:16:07.6	343.0	10.9	2.4	4.6	0.50	
WD0124-257	01:26:55.90	-25:30:53.7	3.0	4.5	3.3	1.4	0.55	
WD0126+101	01:29:24.38	+10:22:59.7	4.0	1.8	1.0	1.9	0.30	
WD0127-050	01:30:23.06	-04:47:57.8	8.1	0.8	1.1	0.8	0.60	
WD0129-205	01:31:39.21	-20:19:59.1	4.1	1.0	2.2	0.5	0.60	
HE0130-2721	01:33:09.08	-27:05:45.0	12.1	2.2	2.2	1.0	0.55	
HE0131+0149	01:34:28.46	+02:04:21.4	392.9	21.6	1.3	16.2	0.50	
WD0133-116	01:36:13.39	-11:20:31.3	4.1	0.5	1.4	0.4	0.50	
WD0135-052	01:37:59.40	-04:59:44.9	4.0	132.4	0.8	159.3	0.20	1, 5
MCT0136-2010	01:38:31.67	-19:54:50.6	6.1	0.9	1.5	0.6	0.70	
WD0137-291	01:40:16.79	-28:52:53.7	2.9	6.1	1.8	3.4	0.50	
WD0140-392	01:42:50.99	-38:59:06.9	2.0	1.1	1.2	0.9	0.55	
WD0145-221	01:47:21.76	-21:56:51.4	2.1	6.5	2.0	3.3	0.60	
HS0145+1737	01:48:21.51	+17:52:13.5	10.9	4.1	1.3	3.3	0.60	
HE0145-0610	01:48:22.27	-05:55:36.5	0.0	9.9	3.8	2.6	0.45	
WD0151+017	01:54:13.88	+02:01:23.5	3.0	0.5	1.4	0.4	0.50	
HE0152-5009	01:54:35.98	-49:55:01.9	12.0	4.3	1.1	3.8	0.50	
WD0155+069	01:57:41.33	+07:12:03.8	121.8	4.1	3.0	1.4	0.50	
HS0200+2449	02:03:45.80	+25:04:09.1	120.7	0.6	2.0	0.3	0.60	
WD0204-233	02:06:45.10	-23:16:14.0	2.0	0.1	1.0	0.1	0.45	
HE0204-4213	02:06:49.89	-41:59:25.8	4.8	0.9	3.0	0.3	0.55	
WD0205-304	02:07:40.86	-30:10:59.6	373.1	1.5	1.2	1.3	0.65	
HE0205-2945	02:08:08.00	-29:31:38.8	357.0	0.5	2.7	0.2	0.35	
HE0210-2012	02:13:01.93	-19:58:35.2	353.0	0.7	1.1	0.7	0.65	
HE0211-2824	02:13:56.66	-28:10:17.8	61.9	1.1	1.0	1.1	0.55	
WD0212-231	02:14:21.26	-22:54:49.1	79.0	10.0	3.8	2.6	0.65	
HE0219-4049	02:21:19.69	-40:35:29.7	6.0	8.2	2.2	3.8	0.55	

Table 1 – continued

Name	RA	Dec	Δt [d]	ΔRV_{\max} [km s ⁻¹]	σ [km s ⁻¹]	N_{σ}	M_1 [M _⊙]	Comments
HE0221-2642	02:23:29.40	-26:29:19.7	226.3	14.0	5.9	2.4	0.55	
HE0221-0535	02:23:59.88	-05:21:45.9	0.9	14.3	2.0	7.3	0.60	
HE0225-1912	02:27:41.43	-18:59:24.5	7.1	48.1	3.1	15.5	0.55	1
HS0225+0010	02:27:55.50	+00:23:39.1	101.7	3.4	1.4	2.4	0.50	
WD0226-329	02:28:27.70	-32:42:35.9	5.0	4.7	1.1	4.1	0.55	
WD0227+050	02:30:16.66	+05:15:50.7	119.7	2.5	0.7	3.7	0.65	
WD0231-054	02:34:07.73	-05:11:39.6	2.9	2.7	1.8	1.5	0.90	
HE0246-5449	02:48:07.16	-54:36:44.9	1.9	0.8	1.6	0.5	0.60	
WD0250-026	02:52:51.05	-02:25:17.4	70.9	1.3	1.5	0.9	0.50	
WD0250-007	02:53:32.29	-00:33:45.3	18.9	1.5	2.8	0.5	0.40	
WD0252-350	02:54:37.25	-34:49:56.6	1.1	3.2	1.0	3.1	0.45	
WD0255-705	02:56:16.90	-70:22:17.7	2.0	3.2	3.4	1.0	0.50	
HE0256-1802	02:58:59.54	-17:50:20.3	78.9	0.8	2.7	0.3	0.55	
HE0257-2104	02:59:52.65	-20:52:49.6	78.9	0.8	2.0	0.4	0.55	
HE0300-2313	03:02:36.69	-23:01:52.0	1.1	7.4	2.2	3.3	0.85	
WD0302+027	03:04:37.40	+02:56:56.6	1.9	4.3	4.3	1.0	0.50	
HE0303-2041	03:06:04.96	-20:29:31.1	6.1	1.4	1.8	0.8	0.55	
HE0305-1145	03:08:10.25	-11:33:45.7	1.0	0.8	2.6	0.3	0.60	
WD0307+149	03:09:53.95	+15:05:22.1	1.0	7.9	2.7	2.9	0.55	
HS0307+0746	03:10:09.13	+07:57:32.6	135.7	2.6	2.7	1.0	0.50	
WD0310-688	03:10:30.99	-68:36:03.3	74.8	1.6	0.5	3.2	0.70	
HE0308-2305	03:11:07.24	-22:54:05.6	2.0	1.4	1.9	0.8	0.90	
WD0308+188	03:11:49.22	+19:00:55.5	117.8	2.7	1.0	2.8	0.50	
HS0309+1001	03:12:34.96	+10:12:27.2	198.3	8.9	2.9	3.1	0.45	
HS0315+0858	03:17:43.18	+09:09:55.2	0.9	2.9	1.4	2.1	0.55	
HE0315-0118	03:18:13.31	-01:07:13.1	2.0	7.4	2.3	3.2	0.50	1
HE0317-2120	03:19:27.22	-21:09:13.2	1.0	0.0	1.6	0.0	0.50	
WD0318-021	03:20:58.77	-01:59:59.5	2.0	0.5	1.7	0.3	0.50	
HE0320-1917	03:22:31.91	-19:06:47.8	1.0	70.4	1.2	61.1	0.30	10
HE0324-2234	03:26:26.88	-22:24:15.0	193.4	1.6	1.5	1.0	0.60	
HE0324-0646	03:26:39.97	-06:36:05.2	5.0	4.5	1.1	4.2	0.65	
HE0324-1942	03:27:05.02	-19:32:23.8	0.9	21.4	3.7	5.8	0.80	1
HE0325-4033	03:27:43.92	-40:23:26.1	0.9	26.8	1.5	17.4	0.55	
WD0326-273	03:28:48.81	-27:19:01.7	3.0	179.3	1.2	151.2	0.35	3
HE0330-4736	03:32:03.98	-47:25:57.7	6.1	3.3	1.5	2.2	0.60	
WD0330-009	03:32:36.90	-00:49:36.6	116.9	1.6	4.8	0.3	0.55	
HE0333-2201	03:36:02.77	-21:51:21.5	34.9	2.7	1.0	2.8	0.70	
HE0336-0741	03:38:26.79	-07:31:54.6	2.0	1.0	1.9	0.5	0.65	
WD0336+040	03:38:56.21	+04:09:43.0	155.8	0.8	2.1	0.4	0.40	
HS0337+0939	03:39:58.55	+09:49:11.3	134.8	3.0	1.9	1.6	0.50	
HE0338-3025	03:40:18.33	-30:15:36.0	1.0	1.7	1.8	0.9	0.55	
WD0341+021	03:44:10.77	+02:15:29.9	201.2	117.1	2.6	44.7	0.30	
WD0344+073	03:46:51.42	+07:28:01.9	215.3	91.3	1.5	60.2	0.35	
HS0344+0944	03:46:52.31	+09:53:56.1	134.8	8.9	2.4	3.7	0.75	
HE0344-1207	03:47:06.71	-11:58:08.5	1.0	11.1	3.1	3.5	0.55	
HS0345+1324	03:48:39.58	+13:33:29.3	155.7	4.3	2.8	1.6	0.75	
HS0346+0755	03:49:15.29	+08:04:53.6	21.0	2.0	2.3	0.9	0.45	
HE0348-4445	03:49:59.27	-44:36:27.4	2.1	1.0	2.6	0.4	0.70	
HE0348-2404	03:50:38.82	-23:55:45.2	1.0	2.1	1.2	1.7	0.55	
HE0349-2537	03:51:41.37	-25:28:16.6	34.9	4.8	3.7	1.3	0.55	
WD0352+052	03:54:41.09	+05:23:19.4	196.3	2.1	3.2	0.6	0.45	
WD0352+018	03:54:43.47	+01:58:41.4	206.2	0.4	3.7	0.1	0.55	
WD0352+096	03:55:22.02	+09:47:17.5	214.2	0.6	1.1	0.6	0.70	
HE0358-5127	03:59:38.30	-51:18:41.5	3.0	3.8	1.6	2.5	0.60	
HS0400+1451	04:03:42.08	+14:59:28.9	201.2	2.7	1.7	1.6	0.85	
HE0403-4129	04:05:30.11	-41:21:10.2	3.0	3.1	3.1	1.0	0.60	
WD0407+179	04:10:10.33	+18:02:24.0	21.0	2.2	1.1	2.0	0.50	
WD0408-041	04:11:02.17	-03:58:22.2	352.0	2.3	1.6	1.5	0.55	
HE0409-5154	04:11:10.33	-51:46:50.8	363.0	8.5	3.0	2.8	0.55	
HE0410-1137	04:12:28.99	-11:30:08.3	4.0	40.9	1.4	28.7	0.50	1

Table 1 – *continued*

Name	RA	Dec	Δt [d]	ΔRV_{\max} [km s ⁻¹]	σ [km s ⁻¹]	N_{σ}	M_1 [M _⊙]	Comments
WD0410+117	04:12:43.60	+11:51:48.5	325.1	0.6	1.0	0.6	0.60	
HS0412+0632	04:14:58.36	+06:40:07.0	333.1	1.2	0.9	1.3	0.55	
HE0414-4039	04:16:02.87	-40:32:11.7	6.0	6.6	2.8	2.3	0.65	
WD0416-550	04:17:11.51	-54:57:47.9	16.0	6.6	1.8	3.6	0.30	
HE0416-3852	04:18:04.14	-38:45:20.6	6.0	2.3	2.1	1.1	0.75	
HE0416-1034	04:18:47.84	-10:27:09.6	28.9	3.6	1.8	2.0	0.60	
HE0417-3033	04:19:22.07	-30:26:44.0	261.2	10.2	3.1	3.3	0.50	
HE0418-5326	04:19:24.83	-53:19:17.4	18.0	1.5	4.3	0.3	0.55	
HE0418-1021	04:21:12.03	-10:14:09.0	260.2	2.6	2.3	1.1	0.80	
WD0421+162	04:23:55.81	+16:21:13.9	307.1	2.0	1.8	1.1	0.70	
HE0425-2015	04:27:39.77	-20:09:15.2	2.1	5.6	3.2	1.7	0.75	
WD0425+168	04:28:39.48	+16:58:10.4	11.0	0.0	1.3	0.0	0.65	
HE0426-1011	04:28:42.32	-10:04:48.9	202.3	3.7	1.4	2.7	0.70	
HE0426-0455	04:29:26.32	-04:48:46.7	3.9	0.5	1.1	0.4	0.60	
WD0431+126	04:33:45.08	+12:42:40.4	1.0	1.8	1.6	1.2	0.60	
HE0436-1633	04:38:47.33	-16:27:21.4	225.3	2.6	1.0	2.5	0.60	
WD0437+152	04:39:52.97	+15:19:44.0	4.0	2.0	1.7	1.2	0.40	
WD0446-789	04:43:46.67	-78:51:50.2	3.0	0.4	1.0	0.4	0.50	
HE0452-3429	04:54:05.85	-34:25:05.9	6.9	5.2	2.3	2.2	0.50	
HE0452-3444	04:54:23.69	-34:39:48.7	32.8	0.5	1.7	0.3	0.55	
HE0456-2347	04:58:51.47	-23:42:55.7	16.1	3.2	2.7	1.2	0.50	
HE0507-1855	05:09:20.47	-18:51:17.3	2.0	0.1	2.8	0.0	0.80	
HS0507+0434B	05:10:13.59	+04:38:54.0	391.9	1.9	2.8	0.7	0.55	
HS0507+0434A	05:10:14.01	+04:38:37.4	399.8	1.3	1.3	1.0	0.55	
HE0508-2343	05:10:39.43	-23:40:10.1	2.0	2.8	1.9	1.5	0.45	
WD0509-007	05:12:06.51	-00:42:07.2	456.9	2.4	3.2	0.8	0.45	
WD0511+079	05:14:03.61	+08:00:14.5	352.1	2.3	2.3	1.0	0.20	
HE0516-1804	05:19:04.27	-18:01:29.1	1.0	22.3	2.7	8.2	0.55	13
HE0532-5605	05:33:06.70	-56:03:53.3	1.0	1.0	3.2	0.3	0.70	
WD0549+158	05:52:27.63	+15:53:13.1	218.3	6.0	1.5	4.1	0.60	
WD0556+172	05:59:44.95	+17:12:03.9	30.9	7.5	2.0	3.7	0.80	
WD0558+165	06:01:17.67	+16:31:37.2	30.9	3.2	1.3	2.4	0.70	
WD0612+177	06:15:18.67	+17:43:40.1	1.9	1.5	1.1	1.4	0.50	
WD0659-063	07:01:55.00	-06:27:48.7	10.0	7.7	1.5	5.2	0.20	
WD0710+216	07:13:21.61	+21:34:06.8	1.9	0.4	1.6	0.3	0.45	
WD0732-427	07:33:37.84	-42:53:58.8	24.9	2.9	1.3	2.2	0.65	
WD0810-728	08:09:31.99	-72:59:17.2	0.0	4.2	3.3	1.3	0.65	
WD0839-327	08:41:32.62	-32:56:34.8	25.0	0.5	0.8	0.6	0.40	
WD0839+231	08:42:53.06	+23:00:25.8	4.9	4.1	1.7	2.5	0.45	
WD0852+192	08:55:30.73	+19:04:37.8	12.9	0.1	1.9	0.1	0.55	
WD0858+160	09:01:33.46	+15:51:43.3	25.9	1.1	1.3	0.8	0.50	
WD0908+171	09:11:24.05	+16:54:11.5	306.2	1.1	2.0	0.5	0.65	
WD0911-076	09:14:22.39	-07:51:25.6	3.0	1.5	1.5	1.0	0.70	
WD0922+162A	09:25:13.55	+16:01:44.7	4.9	2.3	3.4	0.7	0.75	
WD0922+183	09:25:18.37	+18:05:34.3	307.2	9.2	6.1	1.5	0.70	
WD0928-713	09:29:08.65	-71:34:02.8	343.1	4.2	1.4	3.1	0.50	
HS0926+0828	09:29:36.53	+08:15:46.8	334.0	6.7	7.3	0.9	0.55	
HS0929+0839	09:32:29.85	+08:26:37.5	26.8	3.2	1.9	1.7	0.60	
HS0937+0130	09:39:58.67	+01:16:38.2	280.2	2.8	3.0	0.9	0.90	
WD0937-103	09:40:11.96	-10:34:25.1	4.9	7.4	1.5	5.0	0.90	
WD0939-153	09:41:56.22	-15:32:14.6	3.0	0.1	1.1	0.1	0.55	
HS0940+1129	09:43:14.38	+11:16:11.4	26.8	2.9	1.7	1.7	0.65	
HS0943+1401	09:46:31.60	+13:47:35.8	31.8	8.6	3.7	2.3	0.75	
HS0944+1913	09:47:31.67	+18:59:12.7	31.8	1.9	0.8	2.5	0.55	
HS0949+0935	09:51:48.94	+09:21:12.6	63.9	6.3	3.1	2.0	0.65	
HS0949+0823	09:51:56.17	+08:09:33.7	0.0	8.9	2.3	3.9	0.50	
WD0950+077	09:52:59.15	+07:31:08.3	347.1	0.5	1.3	0.4	0.55	
WD0951-155	09:53:40.36	-15:48:56.6	3.0	5.1	1.8	2.9	0.55	
WD0954+134	09:57:18.99	+13:12:57.0	1.0	4.8	2.3	2.1	0.45	
WD0955+247	09:57:48.37	+24:32:55.5	12.0	2.6	1.1	2.4	0.50	

Table 1 – continued

Name	RA	Dec	Δt [d]	ΔRV_{\max} [km s ⁻¹]	σ [km s ⁻¹]	N_{σ}	M_1 [M _⊙]	Comments
WD0956+045	09:58:37.24	+04:21:31.0	22.0	0.3	4.6	0.1	0.70	
WD0956+020	09:58:50.49	+01:47:23.5	3.1	1.8	1.1	1.7	0.60	
WD1003-023	10:05:51.54	-02:34:19.5	22.0	0.0	1.6	0.0	0.75	
HS1003+0726	10:06:23.08	+07:12:12.6	238.1	5.8	4.4	1.3	0.50	
WD1010+043	10:13:12.78	+04:05:12.8	1.0	9.9	4.4	2.2	0.60	
HE1012-0049	10:15:11.75	-01:04:17.1	25.9	1.9	2.0	1.0	0.65	
HS1013+0321	10:15:48.15	+03:06:46.8	245.1	1.5	1.8	0.8	0.55	
WD1013-010	10:16:07.01	-01:19:18.7	20.9	29.0	2.3	12.6	0.25	12
WD1015-216	10:17:26.67	-21:53:43.4	25.8	2.9	2.6	1.1	0.60	
WD1015+161	10:18:03.84	+15:51:58.3	4.9	0.5	1.0	0.5	0.65	
WD1017-138	10:19:52.45	-14:07:35.5	269.0	4.2	2.8	1.5	0.60	
WD1017+125	10:19:56.02	+12:16:29.9	15.1	5.9	2.2	2.7	0.55	
WD1019+129	10:22:28.77	+12:41:59.4	15.0	3.6	1.1	3.2	0.65	
WD1020-207	10:22:43.83	-21:00:02.1	25.8	2.7	1.2	2.3	0.65	
WD1026+023	10:29:09.87	+02:05:49.7	408.9	0.4	1.0	0.4	0.65	
WD1031-114	10:33:42.79	-11:41:40.4	2.0	1.6	1.0	1.7	0.55	
HS1043+0258	10:46:23.34	+02:42:35.6	20.9	1.4	2.1	0.7	0.55	
WD1049-158	10:52:20.69	-16:08:05.9	229.2	0.9	1.3	0.7	0.75	
WD1053-550	10:55:13.77	-55:19:05.8	25.0	2.4	0.7	3.3	0.65	
WD1053-290	10:55:40.04	-29:19:53.4	23.9	3.4	1.6	2.2	0.50	
HS1053+0844	10:55:51.54	+08:28:46.6	4.9	3.8	1.9	2.0	0.65	
WD1056-384	10:58:20.19	-38:44:26.5	25.0	0.6	1.4	0.4	0.60	
WD1058-129	11:01:12.28	-13:14:42.7	166.7	2.3	2.6	0.9	1.00	
HS1102+0934	11:04:36.76	+09:18:22.7	320.9	77.1	1.7	45.9	0.45	9
WD1102-183	11:04:47.08	-18:37:15.2	429.9	2.8	1.2	2.3	0.40	
HS1102+0032	11:05:15.33	+00:16:26.3	264.0	4.0	2.9	1.4	0.80	
WD1105-048	11:07:59.98	-05:09:27.3	269.1	3.1	0.6	5.1	0.50	
HS1115+0321	11:17:46.18	+03:04:51.3	263.1	1.7	1.3	1.3	0.60	
WD1116+026	11:19:12.55	+02:20:30.9	20.9	1.0	1.5	0.6	0.55	
HE1117-0222	11:19:34.66	-02:39:06.3	25.0	6.3	1.0	6.4	0.60	
WD1121+216	11:24:13.08	+21:21:34.8	38.9	0.0	1.0	0.0	0.25	
WD1122-324	11:24:35.62	-32:46:25.7	25.9	0.2	1.7	0.1	0.60	
HE1124+0144	11:26:49.74	+01:27:56.4	1.0	1.2	1.6	0.7	0.55	
WD1124-293	11:27:09.32	-29:40:11.8	23.9	2.5	4.8	0.5	0.50	
WD1124-018	11:27:21.33	-02:08:37.7	1.9	101.9	3.0	34.0	0.50	
WD1125-025	11:28:14.50	-02:50:27.3	0.9	2.3	3.7	0.6	0.75	
WD1126-222	11:29:11.64	-22:33:44.4	25.9	3.3	3.0	1.1	0.55	
WD1129+071	11:32:03.58	+06:55:07.9	6.0	2.0	1.1	1.7	0.65	
WD1129+155	11:32:27.46	+15:17:29.1	4.9	0.9	1.2	0.8	0.75	
WD1130-125	11:33:19.50	-12:49:01.2	1.9	7.8	3.9	2.0	0.80	
HS1136+0326	11:39:26.64	+03:10:19.7	0.9	5.6	2.2	2.6	0.55	
WD1144-246	11:47:20.13	-24:54:56.7	24.9	1.4	2.1	0.7	0.35	
HS1144+1517	11:47:25.13	+15:00:38.7	2.0	0.6	2.4	0.3	0.50	
WD1145+187	11:48:03.18	+18:30:46.6	4.9	0.7	1.4	0.5	0.55	
WD1147+255	11:50:20.18	+25:18:32.6	6.1	1.9	1.7	1.1	0.45	
WD1149+057	11:51:54.29	+05:28:38.3	21.8	4.0	2.8	1.4	0.50	
WD1150-153	11:53:15.37	-15:36:36.8	25.9	5.5	2.8	2.0	0.60	
HE1152-1244	11:54:34.91	-13:01:16.8	27.0	0.5	0.9	0.6	0.50	
HS1153+1416	11:55:59.76	+14:00:13.3	27.0	7.8	3.1	2.5	0.55	
WD1159-098	12:02:07.71	-10:04:40.8	3.0	0.8	1.3	0.6	0.75	
WD1201-001	12:03:47.53	-00:23:11.8	3.0	0.0	1.6	0.0	0.80	
WD1202-232	12:05:26.80	-23:33:13.6	23.9	0.1	0.7	0.1	0.45	
WD1204-322	12:06:47.63	-32:34:33.8	23.9	6.6	1.6	4.1	0.65	
WD1204-136	12:06:56.43	-13:53:53.6	23.9	4.7	1.5	3.1	0.60	
HS1204+0159	12:07:29.51	+01:42:50.6	1.0	11.3	4.2	2.7	0.50	
WD1207-157	12:10:09.34	-16:00:40.4	3.0	0.3	1.2	0.2	0.55	
WD1210+140	12:12:33.89	+13:46:25.1	0.9	133.1	1.8	72.6	0.30	4
WD1216+036	12:18:41.15	+03:20:21.7	11.0	0.0	1.5	0.0	0.50	
WD1220-292	12:23:05.17	-29:32:28.9	1.1	0.9	1.1	0.8	0.70	
HE1225+0038	12:28:07.72	+00:22:19.6	25.0	4.4	1.6	2.7	0.50	

Table 1 – *continued*

Name	RA	Dec	Δt [d]	ΔRV_{\max} [km s ⁻¹]	σ [km s ⁻¹]	N_{σ}	M_1 [M _⊙]	Comments
WD1229-012	12:31:34.46	-01:32:08.5	2.0	0.3	0.9	0.4	0.55	
WD1230-308	12:33:00.67	-31:08:36.4	2.0	6.2	2.8	2.2	0.80	
WD1231-141	12:33:36.89	-14:25:08.6	2.0	5.0	1.7	3.0	0.70	
WD1233-164	12:36:14.02	-16:41:53.5	270.3	14.1	3.9	3.7	0.75	
WD1236-495	12:38:50.02	-49:48:01.1	24.0	3.3	1.8	1.8	0.90	
WD1237-028	12:40:09.66	-03:10:14.8	37.0	0.1	1.6	0.0	0.70	
WD1241-010	12:44:28.66	-01:18:59.6	1.9	5.8	1.0	6.0	0.35	14
HS1243+0132	12:45:38.74	+01:16:16.1	263.1	2.6	5.4	0.5	0.60	
WD1244-125	12:47:26.88	-12:48:42.0	42.8	1.7	1.2	1.4	0.60	
HE1247-1130	12:49:54.26	-11:47:00.2	6.2	2.7	4.9	0.6	0.55	
HS1249+0426	12:52:15.19	+04:10:43.0	33.0	7.6	2.6	2.9	0.50	
WD1249+160	12:52:17.15	+15:44:43.4	1.8	1.9	1.3	1.4	0.30	
WD1249+182	12:52:23.34	+17:56:53.9	1.0	2.3	2.6	0.9	0.55	
HE1252-0202	12:54:58.10	-02:18:36.7	2.9	6.4	2.2	2.9	0.65	
WD1254+223	12:57:02.33	+22:01:52.7	1.0	5.6	3.2	1.7	0.45	
WD1257+047	12:59:50.35	+04:31:26.6	2.0	0.5	1.8	0.3	0.60	
WD1257+032	12:59:56.69	+02:55:56.2	3.0	0.4	1.4	0.3	0.65	
HE1258+0123	13:01:10.50	+01:07:39.9	24.1	0.6	2.6	0.2	0.45	
HE1307-0059	13:09:41.67	-01:15:05.9	3.0	0.2	2.0	0.1	0.75	
HS1308+1646	13:11:06.06	+16:31:03.4	26.0	0.2	3.7	0.0	0.60	
WD1308-301	13:11:17.52	-30:25:57.6	15.9	0.1	0.8	0.1	0.55	
WD1310-305	13:13:41.59	-30:51:33.7	1.0	1.9	1.6	1.2	0.65	
WD1314-153	13:16:43.59	-15:35:58.7	1.0	2.4	1.3	1.9	0.55	
WD1314-067	13:17:18.46	-06:59:28.1	1.2	3.1	1.7	1.9	0.55	
HE1315-1105	13:17:47.29	-11:21:06.2	26.1	0.9	1.1	0.9	0.50	
WD1323-514	13:26:09.62	-51:41:37.9	24.0	2.3	1.1	2.2	0.60	
HE1325-0854	13:28:23.90	-09:09:53.0	2.0	2.2	0.8	2.6	0.55	
HE1326-0041	13:29:24.69	-00:56:43.9	2.9	3.7	1.7	2.2	0.55	
WD1326-236	13:29:24.92	-23:52:18.1	3.0	2.7	1.7	1.6	0.60	
WD1327-083	13:30:13.58	-08:34:30.2	302.1	0.3	0.5	0.6	0.50	
WD1330+036	13:33:17.80	+03:21:00.2	2.9	3.7	1.2	3.2	0.55	
WD1332-229	13:35:10.47	-23:10:38.3	2.0	3.0	2.3	1.3	0.70	
HS1334+0701	13:36:33.67	+06:46:26.8	309.2	13.1	2.0	6.5	0.40	
WD1334-160	13:36:59.29	-16:19:44.1	3.0	0.7	1.3	0.5	0.80	
WD1334-678	13:38:08.11	-68:04:37.4	289.0	5.0	2.5	2.0	0.40	
HE1335-0332	13:38:22.72	-03:47:19.5	3.0	8.0	3.6	2.2	0.90	
HS1338+0807	13:41:27.63	+07:52:29.5	59.9	0.3	2.7	0.1	0.50	
WD1342-237	13:45:46.58	-23:57:11.0	3.0	8.3	2.2	3.9	0.55	
WD1344+106	13:47:24.45	+10:21:36.6	311.0	0.8	1.1	0.8	0.20	
WD1348-273	13:51:22.84	-27:33:59.1	1.0	4.4	3.2	1.4	0.45	
WD1349+144	13:51:54.06	+14:09:44.2	1.1	84.3	2.7	30.7	0.55	1, 8
WD1356-233	13:59:07.97	-23:33:28.7	3.0	3.9	1.1	3.6	0.55	
WD1401-147	14:03:57.16	-15:01:10.4	3.0	1.5	2.4	0.6	0.60	
WD1411+135	14:13:58.22	+13:19:19.3	59.9	2.3	2.3	1.0	0.70	
WD1412-109	14:15:07.75	-11:09:24.2	3.0	0.6	2.6	0.2	0.60	
HE1413+0021	14:16:00.21	+00:07:59.3	2.9	0.6	1.7	0.3	0.65	
HE1414-0848	14:16:52.07	-09:02:03.8	395.9	238.4	4.2	57.3	0.40	1, 2
WD1418-088	14:20:54.82	-09:05:08.7	3.0	2.5	1.5	1.7	0.45	
WD1420-244	14:23:26.25	-24:43:29.4	2.9	4.4	2.2	2.0	0.80	
WD1422+095	14:24:39.24	+09:17:12.7	3.0	0.5	1.6	0.3	0.55	
WD1426-276	14:29:27.38	-27:51:01.3	0.9	1.9	1.3	1.5	0.60	
HS1430+1339	14:33:05.47	+13:26:32.4	3.0	5.9	3.1	1.9	0.60	
WD1431+153	14:34:06.80	+15:08:17.9	6.0	1.4	1.3	1.1	0.55	
HS1432+1441	14:35:20.85	+14:28:41.3	5.0	2.5	1.7	1.5	0.50	
HE1441-0047	14:44:33.85	-00:59:59.5	2.9	3.9	3.9	1.0	0.65	
HS1447+0454	14:50:09.91	+04:41:45.7	59.0	3.1	1.1	2.8	0.55	
WD1448+077	14:50:49.46	+07:33:32.9	323.0	3.6	1.1	3.1	0.55	
WD1449+168	14:52:11.37	+16:38:03.5	6.0	3.0	1.7	1.7	0.50	
WD1451+006	14:53:50.48	+00:25:29.3	2.9	2.7	1.8	1.5	0.55	
WD1457-086	14:59:52.99	-08:49:29.5	2.9	1.9	2.0	0.9	0.55	

Table 1 – continued

Name	RA	Dec	Δt [d]	ΔRV_{\max} [km s ⁻¹]	σ [km s ⁻¹]	N_{σ}	M_1 [M _⊙]	Comments
WD1500-170	15:03:14.45	-17:11:56.7	3.0	5.2	3.3	1.5	0.65	
WD1501+032	15:04:23.92	+03:02:30.5	3.0	0.5	1.0	0.5	0.55	
WD1503-093	15:06:19.44	-09:30:20.9	5.0	1.3	1.7	0.7	0.60	
WD1507-105	15:10:29.08	-10:45:19.8	5.0	5.1	2.2	2.3	0.30	
WD1511+009	15:14:21.31	+00:47:52.3	3.0	4.1	3.1	1.3	0.55	
WD1515-164	15:18:35.07	-16:37:29.2	3.0	1.1	1.3	0.8	0.70	
HS1517+0814	15:20:06.00	+08:03:27.4	35.8	1.7	1.2	1.4	0.45	
HE1518-0344	15:20:46.03	-03:54:52.2	1.0	0.2	3.9	0.1	0.60	
HE1518-0020	15:21:30.87	-00:30:54.7	4.0	7.1	0.9	7.7	0.50	
HE1522-0410	15:25:12.26	-04:21:29.3	16.9	7.2	3.0	2.4	0.55	
HS1527+0614	15:29:41.47	+06:04:01.9	35.8	3.1	0.9	3.5	0.60	
WD1527+090	15:29:50.41	+08:55:46.6	29.0	3.3	1.3	2.6	0.55	
WD1524-749	15:30:36.64	-75:05:24.2	16.0	2.2	1.8	1.2	0.50	
WD1531-022	15:34:06.08	-02:27:07.3	25.1	1.2	1.2	1.0	0.80	
WD1537-152	15:40:23.77	-15:23:43.2	4.0	6.0	1.4	4.3	0.70	
WD1539-035	15:42:14.15	-03:41:31.4	5.0	2.0	1.5	1.3	0.60	
WD1547+057	15:49:34.93	+05:35:15.9	1.0	2.6	2.3	1.1	0.85	
WD1548+149	15:51:15.52	+14:46:58.3	53.9	2.9	2.1	1.4	0.55	
WD1555-089	15:58:04.83	-09:08:06.9	3.0	2.1	1.1	2.0	0.55	
WD1609+135	16:11:25.67	+13:22:17.1	4.0	0.4	1.0	0.3	0.75	
WD1609+044	16:11:49.11	+04:19:38.0	28.0	3.7	2.0	1.8	0.55	
HS1609+1426	16:12:06.51	+14:19:05.8	48.0	3.1	1.3	2.5	0.50	
WD1614+136	16:16:52.31	+13:34:21.5	0.9	0.6	0.9	0.6	0.30	
WD1614-128	16:17:28.02	-12:57:45.6	1.8	0.1	1.3	0.1	0.60	
WD1615-154	16:17:55.24	-15:35:52.7	1.8	2.5	1.5	1.6	0.70	
HS1616+0247	16:19:18.91	+02:40:14.1	98.9	6.5	2.0	3.2	0.60	
WD1625+093	16:27:53.57	+09:12:14.8	24.9	5.4	2.1	2.5	0.30	
WD1636+057	16:38:54.53	+05:40:40.1	25.9	0.6	2.1	0.3	0.70	
WD1640+113	16:42:54.87	+11:16:40.6	8.0	1.3	2.6	0.5	0.75	
HS1641+1124	16:43:54.12	+11:18:50.2	0.9	2.6	1.6	1.6	0.60	
HS1646+1059	16:48:40.74	+10:53:52.8	20.0	2.9	2.1	1.4	0.55	
HS1648+1300	16:51:02.78	+12:55:12.7	1.0	0.8	1.4	0.6	0.50	
WD1655+215	16:57:09.84	+21:26:48.4	20.0	0.7	1.3	0.5	0.45	
HS1705+2228	17:07:08.03	+22:24:30.0	17.0	1.9	1.1	1.7	0.55	
WD1733-544	17:37:00.76	-54:25:56.9	1.0	1.2	2.9	0.4	0.20	
WD1736+052	17:38:41.72	+05:16:06.3	7.9	9.6	1.5	6.6	0.50	
WD1755+194	17:57:38.92	+19:24:18.5	92.9	5.5	3.9	1.4	0.60	
WD1802+213	18:04:23.53	+21:21:02.5	17.0	1.4	1.6	0.9	0.55	
WD1824+040	18:27:13.13	+04:03:45.9	83.7	96.7	1.1	88.2	0.35	7
WD1834-781	18:42:25.50	-78:05:06.4	7.0	1.7	1.0	1.7	0.65	
WD1845+019	18:47:37.00	+01:57:30.0	32.0	2.8	1.2	2.2	0.55	
WD1857+119	18:59:49.27	+11:58:39.8	9.2	5.8	4.0	1.5	0.45	
WD1911+135	19:13:38.77	+13:36:26.3	1.2	1.3	2.8	0.5	0.55	
WD1914-598	19:18:44.85	-59:46:33.5	32.0	2.6	1.1	2.4	0.70	
WD1918+110	19:20:35.29	+11:10:43.3	1.0	2.4	1.5	1.6	0.65	
WD1932-136	19:35:42.05	-13:30:07.8	1.0	0.2	1.5	0.2	0.60	
WD1943+163	19:45:31.73	+16:27:38.8	17.0	0.7	1.0	0.8	0.65	
WD1952-206	19:55:46.99	-20:31:02.9	7.0	0.4	0.9	0.5	0.60	
WD1953-715	19:58:38.64	-71:23:43.6	1.0	3.6	1.7	2.2	0.70	
WD1959+059	20:02:12.92	+06:07:35.4	25.9	5.1	3.0	1.7	0.60	
WD2007-219	20:10:17.48	-21:46:46.0	23.1	1.3	1.0	1.3	0.50	
WD2014-575	20:18:54.88	-57:21:33.8	5.0	0.1	1.3	0.0	0.65	
WD2018-233	20:21:28.71	-23:08:30.4	83.7	2.9	1.4	2.1	0.55	
WD2020-425	20:23:59.57	-42:24:26.7	23.0	225.9	2.9	77.3	0.75	1
WD2021-128	20:24:42.94	-12:41:48.4	31.9	3.2	2.0	1.6	0.70	
WD2029+183	20:32:02.91	+18:31:15.1	102.8	6.5	1.9	3.4	0.45	
WD2032+188	20:35:13.84	+18:59:21.8	6.0	3.2	2.4	1.3	0.50	15
WD2039-682	20:44:21.35	-68:05:21.4	27.1	2.5	1.4	1.8	0.85	
HS2046+0044	20:48:38.26	+00:56:00.8	16.9	23.8	3.8	6.2	0.70	
WD2046-220	20:49:46.18	-21:54:43.1	83.7	1.0	1.8	0.6	0.50	

Table 1 – *continued*

Name	RA	Dec	Δt [d]	ΔRV_{\max} [km s ⁻¹]	σ [km s ⁻¹]	N_{σ}	M_1 [M _⊙]	Comments
WD2051+095	20:53:43.18	+09:41:14.5	25.8	1.6	1.8	0.8	0.50	
HS2056+0721	20:58:45.03	+07:33:37.5	2.0	1.1	2.1	0.5	0.80	
WD2058+181	21:01:16.50	+18:20:55.4	72.8	0.5	1.4	0.3	0.60	
HS2059+0208	21:01:47.77	+02:20:27.6	17.9	1.5	2.5	0.6	0.65	
WD2059+190	21:02:02.68	+19:12:57.5	1.0	0.3	1.8	0.2	0.20	
WD2115+010	21:17:33.58	+01:15:47.1	1.0	4.7	1.9	2.5	0.50	
WD2122-467	21:25:30.19	-46:30:36.8	58.9	3.0	1.9	1.5	0.75	
HS2132+0941	21:34:50.91	+09:55:19.0	4.0	2.5	1.9	1.3	0.45	
HE2133-1332	21:36:16.18	-13:18:33.0	30.0	2.8	1.0	2.9	0.35	
WD2134+218	21:36:36.15	+22:04:32.8	61.8	3.9	1.3	3.1	0.60	
WD2136+229	21:38:46.21	+23:09:20.9	69.8	4.1	2.2	1.9	0.50	
HE2135-4055	21:38:49.70	-40:41:28.9	2.0	1.0	0.9	1.1	0.60	
WD2137-379	21:40:18.48	-37:42:46.7	1.0	3.7	2.3	1.6	0.55	
HS2138+0910	21:41:03.02	+09:23:45.4	4.0	4.1	1.1	3.8	0.40	
WD2139+115	21:41:28.37	+11:46:22.1	3.1	0.3	1.2	0.2	0.60	
HE2140-1825	21:43:42.73	-18:11:32.6	62.7	1.7	1.0	1.7	0.55	
HS2148+1631	21:51:14.54	+16:45:23.1	1.0	1.1	1.7	0.6	0.55	
HE2148-3857	21:51:19.23	-38:43:04.5	1.0	11.5	4.0	2.9	0.70	
WD2151-307	21:54:53.38	-30:29:19.6	22.1	6.8	2.3	2.9	0.80	
HE2155-3150	21:58:46.08	-31:36:06.5	59.7	4.3	1.6	2.6	0.65	
WD2157+161	21:59:34.35	+16:25:39.0	1.0	0.8	2.5	0.3	0.55	
HE2159-1649	22:02:20.82	-16:34:38.3	256.1	3.8	1.6	2.4	0.65	
WD2200-136	22:03:35.63	-13:26:49.9	368.1	104.0	4.7	22.3	0.45	1
WD2159-754	22:04:21.27	-75:13:25.9	258.1	0.9	1.1	0.8	0.85	
HE2203-0101	22:06:02.44	-00:46:33.5	399.0	6.0	1.6	3.7	0.65	
WD2204+071	22:07:16.20	+07:18:36.0	3.1	3.9	2.4	1.6	0.65	
WD2207+142	22:09:47.19	+14:29:46.6	5.9	1.0	2.0	0.5	0.35	
HE2209-1444	22:12:18.05	-14:29:48.0	287.1	106.3	1.4	75.5	0.60	1, 6
HS2210+2323	22:12:53.48	+23:38:00.4	0.9	2.3	5.5	0.4	0.75	
HS2216+1551	22:18:57.15	+16:06:56.9	1.1	12.4	1.9	6.4	0.65	1
HE2218-2706	22:21:23.91	-26:50:55.2	15.9	2.6	1.2	2.2	0.55	
HE2220-0633	22:22:44.44	-06:17:54.9	397.0	0.3	1.5	0.2	0.60	
HS2220+2146B	22:23:01.64	+22:01:31.0	1.1	1.3	1.3	1.0	0.85	
HE2221-1630	22:24:17.51	-16:15:47.0	290.3	0.1	1.5	0.0	0.55	
HS2225+2158	22:28:11.47	+22:14:15.1	1.0	3.3	2.5	1.3	0.55	
WD2226+061	22:29:08.66	+06:22:46.3	4.9	1.3	3.4	0.4	0.50	
WD2226-449	22:29:19.47	-44:41:39.4	277.2	1.4	0.6	2.5	0.60	
HS2229+2335	22:31:45.45	+23:51:23.9	1.0	3.9	1.5	2.6	0.70	
HE2230-1230	22:33:38.69	-12:15:30.4	64.7	4.8	1.9	2.5	0.55	
HE2231-2647	22:34:02.59	-26:32:21.1	233.3	2.8	2.4	1.2	0.50	
HS2233+0008	22:36:03.20	+00:07:23.9	1.0	3.4	1.3	2.5	0.60	
WD2241-325	22:44:43.23	-32:19:43.7	317.2	1.9	2.7	0.7	0.70	
HS2244+2103	22:46:45.28	+21:19:47.7	0.9	3.1	3.4	0.9	0.60	
WD2248-504	22:51:02.02	-50:11:31.8	7.0	10.1	2.8	3.6	0.60	
HE2251-6218	22:54:59.62	-62:02:10.2	1.0	2.1	1.8	1.1	0.65	
WD2253-081	22:55:49.49	-07:50:03.3	5.0	12.4	1.7	7.5	0.20	
WD2254+126	22:56:46.26	+12:52:49.9	34.8	11.4	4.9	2.3	0.55	
HS2259+1419	23:01:55.18	+14:36:00.5	1.0	1.8	1.1	1.6	0.55	
WD2303+242	23:06:17.70	+24:32:07.5	1.0	0.6	1.7	0.4	0.50	
WD2306+130	23:08:30.58	+13:19:22.7	370.0	3.9	1.5	2.6	0.60	
WD2306+124	23:08:35.07	+12:45:39.0	39.9	5.9	2.1	2.8	0.70	
WD2308+050	23:11:18.05	+05:19:27.9	1.0	11.4	4.3	2.7	0.45	
WD2312-356	23:15:34.95	-35:24:51.8	18.2	3.8	1.1	3.6	0.55	
WD2314+064	23:16:50.36	+06:41:27.6	0.9	1.0	2.8	0.4	0.60	
WD2318+126	23:20:31.30	+12:58:14.5	0.9	1.3	1.6	0.8	0.60	
WD2322+206	23:24:35.22	+20:56:33.9	0.9	2.1	1.1	1.9	0.50	
WD2322-181	23:25:18.40	-17:51:57.8	3.0	2.9	1.4	2.0	0.65	
WD2324+060	23:26:44.55	+06:17:41.4	0.9	1.3	1.2	1.1	0.60	
WD2326+049	23:28:47.74	+05:14:53.5	42.0	5.3	1.1	5.0	0.55	
WD2328+107	23:30:41.79	+11:02:05.0	2.9	0.7	1.3	0.5	0.55	

Table 1 – continued

Name	RA	Dec	Δt [d]	ΔRV_{\max} [km s ⁻¹]	σ [km s ⁻¹]	N_σ	M_1 [M _⊙]	Comments
WD2329-332	23:32:10.90	-33:01:08.1	3.1	1.2	3.5	0.3	0.60	
WD2330-212	23:32:59.48	-20:57:12.1	2.9	55.5	2.6	21.8	0.40	
WD2333-165	23:35:36.59	-16:17:42.5	42.0	1.7	0.6	2.6	0.50	
WD2333-049	23:35:53.96	-04:42:14.8	40.9	2.6	2.7	1.0	0.50	
HE2334-1355	23:37:30.38	-13:38:33.4	2.9	5.1	1.8	2.7	0.35	
WD2336-187	23:38:52.78	-18:26:11.9	3.0	42.1	5.8	7.3	0.25	1
WD2336+063	23:38:58.25	+06:35:28.6	2.9	0.7	1.1	0.6	0.65	
MCT2343-1740	23:46:25.63	-17:24:10.2	0.9	0.2	4.9	0.0	0.55	
MCT2345-3940	23:48:26.42	-39:23:47.4	0.9	2.6	2.2	1.2	0.55	
WD2347+128	23:49:53.51	+13:06:12.5	2.0	8.5	3.8	2.2	0.45	
WD2347-192	23:50:02.96	-18:59:21.9	40.8	1.8	3.5	0.5	0.60	
HE2347-4608	23:50:32.90	-45:51:34.8	10.2	2.3	1.3	1.9	0.45	
WD2348-244	23:51:22.10	-24:08:17.0	39.9	0.2	1.7	0.1	0.50	
WD2349-283	23:52:23.18	-28:03:15.9	39.9	2.1	1.1	2.0	0.50	
WD2350-248	23:53:03.79	-24:32:03.1	41.7	2.5	2.9	0.9	0.85	
WD2350-083	23:53:27.63	-08:04:39.5	63.9	4.0	1.4	2.9	0.55	
WD2351-368	23:54:18.82	-36:33:55.1	4.0	1.6	1.6	1.0	0.55	
WD2354-151	23:57:33.44	-14:54:09.1	41.8	4.7	2.4	1.9	0.35	
HE2356-4513	23:58:57.83	-44:57:13.5	0.0	2.6	1.2	2.2	0.55	

Notes: σ is the root of the summed squares of the RV errors of the two individual RV measurements forming each difference. N_σ is defined as $\Delta RV_{\max}/\sigma$. M_1 is the derived mass for the photometric-primary WD. DWD candidates with $\Delta RV_{\max} > 10 \text{ km s}^{-1}$ are highlighted.

- (1) Double-lined DWD (2) HE1414-0848: $P = 0.5178 \text{ d}$, $M_1 = 0.55 M_\odot$, $M_2 = 0.71 M_\odot$ (Napiwotzki et al. 2002) (3) WD0326-273: $P = 1.8754 \text{ d}$, $M_1 = 0.51 M_\odot$, $M_{2,\min} = 0.59 M_\odot$ (Nelemans et al. 2005) (4) WD1210+140: $P = 0.64194 \text{ d}$, $M_1 = 0.23 M_\odot$, $M_{2,\min} = 0.38 M_\odot$ (Nelemans et al. 2005) (5) WD0135-052: $P = 1.553 \text{ d}$, $M_1 = 0.47 M_\odot$, $M_2 = 0.52 M_\odot$ (Saffer et al. 1988; Bergeron et al. 1989) (6) HE2209-1444: $P = 0.2769 \text{ d}$, $M_1 = 0.58 M_\odot$, $M_2 = 0.58 M_\odot$ (Karl et al. 2003b) (7) WD1824+040: $P = 6.26600 \text{ d}$, $M_1 = 0.428 M_\odot$, $M_{2,\min} = 0.515 M_\odot$ (Morales-Rueda et al. 2005) (8) WD1349+144: $P = 2.2094 \text{ d}$, $M_1 = 0.44 M_\odot$, $M_2 = 0.44 M_\odot$ (Karl et al. 2003a) (9) HS1102+0934: $P = 0.55319 \text{ d}$, $M_1 = 0.46 M_\odot$, $M_{2,\min} = 0.55 M_\odot$ (Brown et al. 2013) (10) HE0320-1917: $P = 0.86492 \text{ d}$, $M_1 = 0.29 M_\odot$, $M_{2,\min} = 0.35 M_\odot$ (Nelemans et al. 2005) (11) WD0032-317: possible 1500 K BD companion, based on weak NIR excess. (12) WD1013-010: $P = 0.43653 \text{ d}$, $M_1 = 0.44 M_\odot$, $M_{2,\min} = 0.38 M_\odot$ (Nelemans et al. 2005) (13) HE0516-1804: possible NIR excess indicating a $T_{\text{eff}} \sim 3000 \text{ K}$ companion with radius $\sim 0.2 R_\odot$. (14) WD1241-010: $P = 3.34741 \text{ d}$, $M_1 = 0.31 M_\odot$, $M_{2,\min} = 0.373 M_\odot$ (Marsh et al. 1995) (15) WD2032+188: $P = 5.0846 \text{ d}$, $M_1 = 0.406 M_\odot$, $M_{2,\min} = 0.469 M_\odot$ (Morales-Rueda et al. 2005)

(A full version of this table appears in the electronic version of the article.)